

Metasurface optical holography

Zi-Lan Deng ^a, Guixin Li ^{b,*}



^a Guangdong Provincial Key Laboratory of Optical Fiber Sensing and Communications, Institute of Photonics Technology, Jinan University, Guangzhou, 510632, China

^b Department of Materials Science and Engineering, Institute for Quantum Science and Engineering, Southern University of Science and Technology, 518055, Shenzhen, China

ARTICLE INFO

Article history:

Received 9 October 2017

Received in revised form

9 November 2017

Accepted 14 November 2017

Available online 1 December 2017

Keywords:

Photonic metasurfaces

Metamaterials

Optical holography

Nanophotonics

ABSTRACT

Photonic metasurface, a 2D array of plasmonic or dielectric optical meta-atoms, provides a versatile and compact platform for manipulating the polarization, phase and amplitude of light. It has been used to design planar optical functional elements such as ultrathin metasurface lens, metasurface waveplates, polarization beam splitter and so on. More generally, metasurface is capable of shaping the general and complex wavefront of light through holography techniques. Compared with conventional techniques, optical holography based on metasurface provides much more flexibilities to control the polarization, view angle, dispersive color crosstalk of holographic images, and thus making the metasurface optics more practical for various applications. In this review, we firstly discuss the concept of metasurface holography based on various phase modulation mechanisms including resonant phase, geometric phase, and propagation phase, etc. Then various holographic multiplexing techniques through degrees of wavelength, polarization, spatial distribution and nonlinear optical processes are summarized. Finally, we envision the future applications of metasurface optical holography from the view of large area fabrication, reconfigurable and dynamic wavefront engineering for 3D displaying, high capacity data storage, information encryption and so on.

© 2017 Elsevier Ltd. All rights reserved.

1. Introduction

Metamaterials composed of artificial building blocks (meta-atoms) at subwavelength scale have been extensively studied for about two decades in the optics community, due to their unprecedented capabilities of controlling the propagating of electromagnetic waves in desired ways that may not be possible with natural materials [1]. In bulk metamaterials, the strong dispersion and loss can significantly degrade their optical performance and thus limit the practical applications. At optical frequencies, the fabrication of bulk metamaterial is challenging due to the critical requirements during precise multilayer stacking. The advent of metasurface, a 2D array of spatially variant meta-atoms provides novel solutions to circumvent the constraints in optical bulk metamaterials. When light impinges on constituent metallic or dielectric meta-atoms of the metasurface, abrupt phase changes that are determined by the geometrical parameters (shape, size, or orientation) of the meta-atoms will be produced. Therefore, any desired phase distribution for arbitrary

wavefront shaping on a metasurface can be realized by designing spatially varying meta-atoms. For example, by designing the phase distribution as a simple linear phase profile with a constant phase gradient $d\Phi/dx$, abnormal refraction and reflection that obeys the generalized Snell's law were demonstrated [2–5]. In a more complicated case, linear phase gradient profile along the azimuthal direction or radial direction can be designed in a cylindrical coordinate system to generate the vortex beams with desired orbital angular momenta [2,4,6–10] or Bessel beams [11]. Using the similar principle, if the phase distribution impinged by the metasurface has a quadratic profile, ultrathin planar lens, one of the most important optical components in imaging systems, can be realized with various numerical apertures and aberration-reduced characteristics [11–18]. In addition, by exploiting the anisotropic scattering properties of meta-atoms, polarizations of light can also be well controlled by metasurfaces with versatile functionalities [19–23]. Most of the above optical metasurfaces are designed by using the analytical forms of phase profiles, their general working principles and applications have been discussed in several review articles [24–28].

As for the general wavefront shaping, it is well known that optical holography is a powerful technique and provide general

* Corresponding author.

E-mail address: [\(G. Li\).](mailto:ligx@sustc.edu.cn)

solutions to wavefront engineering of light beams. Applying metasurface to achieve holographic imaging has attracted increasing attentions in recent years due to its great potentials in producing ultra-compact optical surfaces for data storage, information encryption, microscopy, 3D displays, and so on.

In this review, we mainly focus on the basic concept and the recent progresses of metasurface optical holography. The contents are organized as follows. Firstly, we overview the basic working principles of metasurface holography, including the methods of phase modulation, the mapping schemes from a holographic image to the phase distribution of a metasurface hologram and the design of metasurface structure. Next, we discuss the polarization multiplexing by using meta-holograms in which dual holographic images can be switched to each other by tuning the polarization states of the incident light. Then various wavelength-multiplexed metasurface with versatile functionalities including achromatic focusing, dynamic color displaying, and full-color 3D images are introduced. And next, spatially-multiplexed and nonlinear optical meta-holograms are also summarized. Finally, we outlook both the potential applications and remaining challenges of metasurface optical holography.

2. Basic concept of the metasurface optical holography

2.1. Conventional optical holography

Optical holography, which involves the full recording both the amplitude and phase of a wavefront, is superior to the conventional photography process in which only the amplitude information of light is recorded. Since its invention by Dennis Gabor in 1948 [29], holography techniques have been widely used in various fields, such as interferometry, microscopy, lensless imaging, data storage, 3D display and so on.

2.1.1. Holographic recording methods

At the early stage of holography, the interference method between an object wave and a reference wave is the main recording approach. Along with the rapid development of computation facilities, computer generated holograms (CGHs) [30,31] that record the object information using computational algorithm becomes more popular, as there is no need for a real interference between two waves, and nonexistent virtual 3D objects can also be recorded by the CGHs. As far as the encoding methodologies, the optical holograms can be divided to binary hologram, amplitude- and phase-type holograms [32,33]. Phase-type holograms are widely used due to their high diffraction efficiency and available recording materials. As an arbitrary wavefront usually contains both amplitude and phase information, the amplitude information can be moved out by adding a random diffuser by using the Gerchberg–Saxton (GS) iterative algorithm [34].

2.1.2. Holographic recording materials

The traditional holographic recording medium could be a holographic plate made of emulsion or photo-reduced polymer, which are based on accumulated phase change when light propagates for a wavelength scale distance. So the recording medium is usually a thick layer, which inevitably limits the integration and miniaturization of the optical system. In the application of holographic display, liquid crystal based spatial light modulators (SLMs) is a novel recording medium which enables dynamic image recording and display. However, the performance of SLMs are limited by their large pixel size of several to tens of micrometers. For visible wavelengths, the view angles of SLMs are largely restricted ($\sim 4^\circ$) and there exists quite a lot of unwanted high diffraction orders [35,36].

As we can see, many technological difficulties in conventional optical holography, including the low diffraction efficiency, unwanted diffraction orders, poor quality of the images, mono-color or limited color appearance, and lack of polarization degree of freedom, may hinder its practical applications. Some advanced holography techniques based on surface plasmon resonances [37–42], two-dimensional materials [43,44] and bulk metasurfaces [45,46] emerge in recent years, but they can only partially address the problems of conventional optical holography.

2.2. Principle of metasurface optical holography

Photonic metasurface, as a novel holographic recording medium, provides much more degrees of freedom to encode the holographic information on a miniaturized surface. Due to the subwavelength size of the unit cell, the view angle of a holographic display from the metasurface hologram is much wider ($\sim 60^\circ$) [47] than the conventional holograms based on SLMs. Thanks to the modern nanofabrication technologies, the precise control of geometric parameters of both plasmonic and dielectric metasurfaces provides a facile way to tailor the meta-atom's scattering characteristics at will. This leads to high diffraction efficiency [47], high image fidelity [48] and full-color performances [49,50] of the holographic imaging, which is highly desired for practical applications. In addition, optical holograms based on the various degrees of freedom such as polarization [51–54], spin angular momentum [48,55–57], wavelength [49,50,58–63], wavevector [64–67] and nonlinear optical processes [68–73] have been fully exploited to realize versatile optical functionalities which are very challenging if not impossible in conventional optical holography.

2.2.1. Phase modulation rules of various meta-atoms

The phase modulation mechanisms on metasurfaces rely on the abrupt phase discontinuity caused by the scattering of subwavelength meta-atoms. The abrupt phase can be tailored by varying the geometric parameters (typically the size, shape, and orientation) of the meta-atoms. Different from the traditional holograms which employ the accumulated propagation phase in a thick refractive medium, the phase modulation on metasurface can be achieved by using an ultrathin flat surface, which can largely miniaturize the volume of optical systems.

2.2.1.1. Resonant phase modulation. Fig. 1 shows the relationships between the modulated phase and the geometry of the meta-atom. In the earlier demonstration of metasurfaces [2], both the opening and orientation angles of the V-shaped meta-atoms should be varied according to the scattering amplitude and phase (0– 2π) for cross linear polarizations (Fig. 1a). Similar phase modulation methods were also implemented in terahertz frequency range by using the C-shaped meta-atoms (Fig. 1b), which can independently control both the phase and the amplitude of the electric field of incident wave [74,75]. Fig. 1c shows the phase modulation method by tuning the localized plasmon resonance (LPR) wavelengths through changing the size of the plasmonic nanorods. At the resonance frequency of a plasmonic meta-atom, the phase of the scattered light undergoes a jump of π . By placing a metallic mirror underneath the plasmonic nanorods, the scattered light experiences a doubled resonances and thus introduces a full 2π modulation range with a near flat amplitude profile.

Box 1. Physical mechanisms of resonant phase modulations on metasurfaces. The resonance of the plasmonic or high-index dielectric meta-atoms can be modeled using a Lorentz model. From the coupled model theory [76–78], the reflection

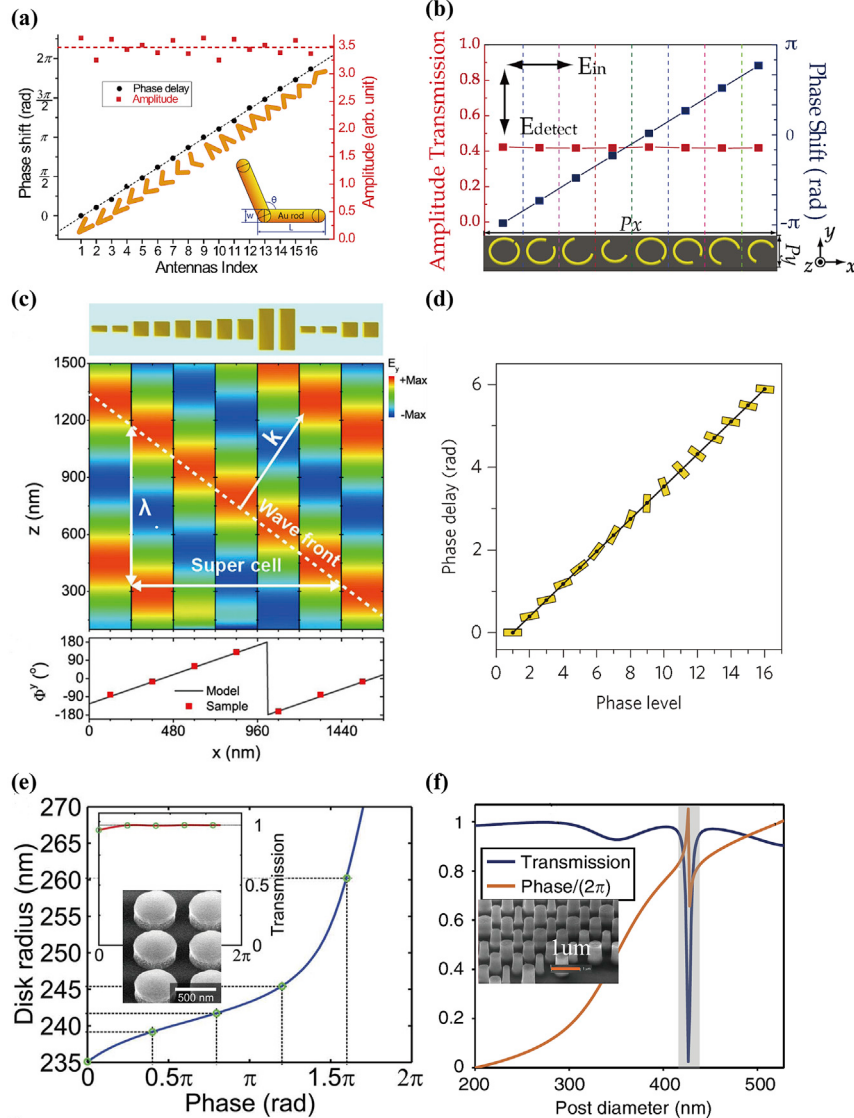


Fig. 1. The relationships between geometry parameters of the metasurface and the modulated phase, for different types of meta-atoms: (a) V-shaped antennas with double resonances [149], (b) C-shaped meta-atom [74,75], (c) resonant metal bars with different sizes [150], (d) metal nanorods with spatially varying orientations [47], (e) Huygens dielectric meta-atoms supporting overlapped electric and magnetic resonances [85], (f) dielectric posts supporting waveguide modes [91].

coefficient r and transmission coefficient t are given by the following equations:

$$r(\omega) = \frac{\gamma}{i(\omega - \omega_{res}) + \gamma}, \quad (1)$$

$$t(\omega) = \frac{i(\omega - \omega_{res})}{i(\omega - \omega_{res}) + \gamma}, \quad (2)$$

where, ω_{res} is the resonance frequency, γ is the damping rate of the meta-atom. The amplitude and phase spectra of $r(\omega)$ and $t(\omega)$ are plotted as blue and green curves in Fig. 2(b, c), respectively. It can be seen that, a phase shift across π is induced near the resonant wavelength in both the reflection and transmission cases (blue and green curves in Fig. 2(c)). To obtain the full phase modulation range of 0- 2π and near unity optical efficiency, the reflection-type metasurface consisting of the meta-atoms/dielectric spacer and a metallic mirror can be utilized (Fig. 2(a)). The reflection coefficient of the tri-layer metasurface can be written as:

$$r'(\omega) = \frac{j(\omega - \omega_{res}) - \gamma}{j(\omega - \omega_{res}) + \gamma}. \quad (3)$$

The amplitude and phase of $r'(\omega)$ are plotted as red curves in Fig. 2(b, c), in which the amplitude is always near-unity, and the phase cross the 0- 2π range near the resonance.

For transmission-type resonant metasurfaces, to obtain the 0- 2π phase modulation with near-unity optical efficiency, impedance matching should be satisfied to eliminate the light reflection. This can be realized by exploiting both the electric and magnetic dipole resonances of a high-index dielectric nanoresonator (Fig. 2(d)). The impedance matching condition is described by:

$$\sqrt{\alpha_m/\alpha_e} = \eta_0, \quad (4)$$

where, η_0 is the impedance of the surrounding medium of the metasurface, and α_m , α_e are the resonant magnetic and electric polarizabilities with a typically Lorentz line shape $\alpha_e = \frac{\alpha_0^e}{\omega_e^2 - \omega^2 - 2i\gamma_e\omega}$,

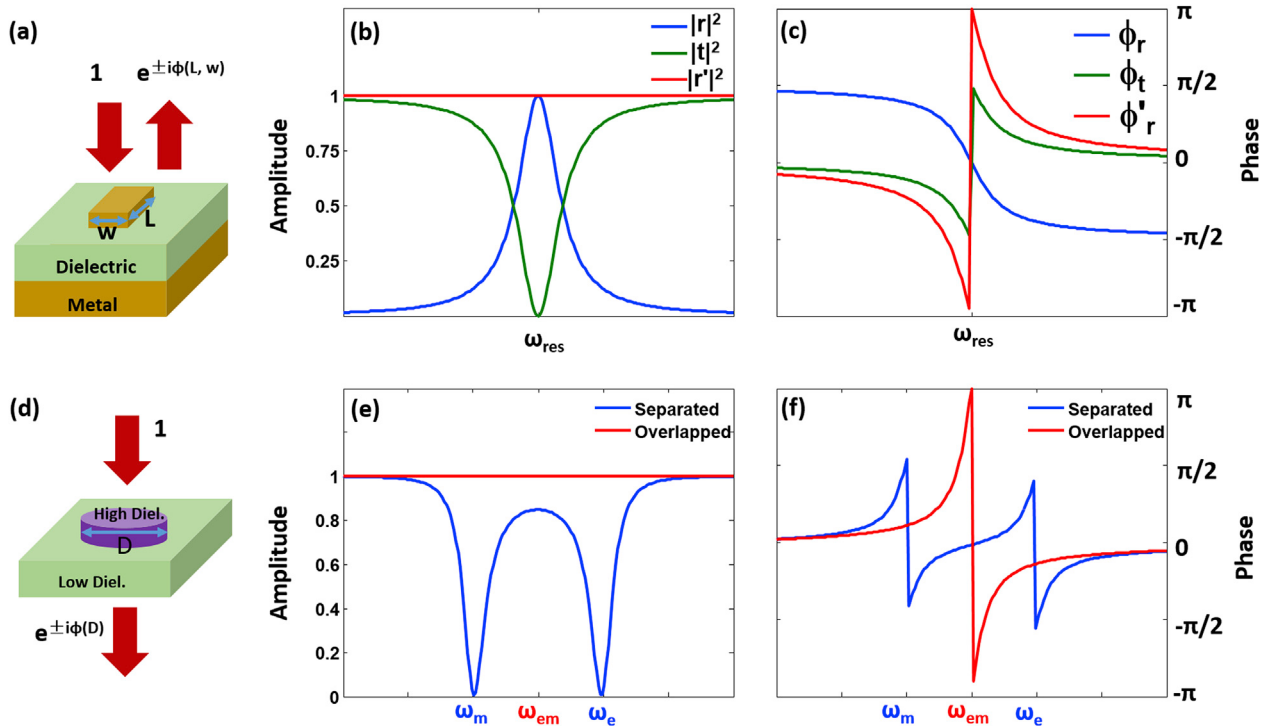


Fig. 2. The physical mechanism of resonant phase. (a) Configuration of metal-dielectric-metal tri-layer plasmonic meta-atom, which can efficiently covert the incident light into the reflected light with a resonant phase $\phi(L, w)$. (b, c) The amplitude and phase of the reflection (blue), transmission (green) for a single layer meta-atom, as well as the reflection (red) coefficients for a tri-layer meta-atom. (d) Huygens type dielectric meta-atom with high refractive index. The electric field of transmitted light has a resonant phase $\phi(D)$. (e–f) Amplitude (e) and phase (f) modulations of two separated electric and magnetic dipole resonances (blue curves) and two overlapped electric and magnetic dipole resonances (red curves), respectively, in the high-index dielectric meta-atom shown in (d).

$\alpha_m = \frac{\alpha_0^m}{\omega_m^2 - \omega^2 - 2i\gamma_m\omega}$, where $\omega_{e,m}$ and $\gamma_{e,m}$ are resonant frequencies and damping rates of the electric and magnetic dipoles, respectively, and $\alpha_0^{e,m}$ are the amplitudes of the resonances. From the coupled model theory, the transmission coefficient can be written as,

$$t_{em} = 1 + \frac{2i\gamma_e\omega}{\omega_e^2 - \omega^2 - 2i\gamma_e\omega} + \frac{2i\gamma_m\omega}{\omega_m^2 - \omega^2 - 2i\gamma_m\omega}. \quad (5)$$

As shown in Fig. 2(e, f), if the electric and magnetic resonances are separated ($\omega_e \neq \omega_m$), the amplitude and phase spectra are the simple superposition of two individual resonant items. In this case, the amplitudes exhibit resonant dips and the phase range only covers $-\pi/2$ to $\pi/2$ (blue curves in Fig. 2(f)). In the overlapped case with $\omega_e = \omega_m$ and $\lambda_e = \lambda_m$, the two resonant modes interfere with each other and the overall transmission efficiency is close to unity for a wide spectral range and the induced phase change can cover the full 2π range (red curves in Fig. 2(e, f)).

2.2.1.2. Geometric pancharatnam-berry (P-B) phase. As shown in Fig. 1d, the geometric P-B phase comes from the spin rotation effect when a circularly polarized light interacts with plasmonic [47] or all-dielectric [14] meta-atoms with optical anisotropy. To some extent, geometric phase is solely determined by the orientation angle of the meta-atom and circular polarization state of incident light. For a meta-atom with in-plane orientation angle of ϕ , the induced geometric phase is simply $2\sigma\phi$ [Box 2], where $\sigma = \pm 1$ represents the left- and right-circular polarizations, which is very convenient for designing complex phase profiles, and thus is widely used in various metasurface holograms with high performances [47–50,79,80].

Box 2. Physical mechanism of geometric P-B phase. The origin of geometric P-B phase can be explained by considering the meta-atom as an anisotropic meta-atom. The light scattering property of the meta-atom can be described by the Jones matrix, (assuming the meta-atom has mirror-symmetry so that the non-orthogonal elements are zero),

$$S(0) = \begin{pmatrix} s_1 e^{i\varphi_1} & 0 \\ 0 & s_2 e^{i\varphi_2} \end{pmatrix}, \quad (6)$$

where $s_1 e^{i\varphi_1}$, $s_2 e^{i\varphi_2}$ are the complex scattering (reflection or transmission) coefficients with respect to the main axis 1 and 2 of the meta-atom (Fig. 3). By rotating the meta-atom with angle ϕ , the Jones matrix of the meta-atom becomes: $S(\phi) = R^\dagger(\phi)S(0)R(\phi)$, where $R(\phi)$ is the rotation matrix. By employing the Pauli's matrices notation $\{\hat{\sigma}_1, \hat{\sigma}_2, \hat{\sigma}_3\}$, we can define two spin-flip operations $\hat{\sigma}_\pm = (\hat{\sigma}_1 \pm i\hat{\sigma}_2)/2$ that satisfies $\hat{\sigma}_\pm |\pm\rangle = 0$, and $\hat{\sigma}_\pm |\mp\rangle = |\pm\rangle$, where $|\pm\rangle$ denotes the spin-up (LCP) and spin-down (RCP) states of light, respectively. The rotation matrix has the form of $R(\phi) = e^{i\phi\sigma_3}$ and the Jones matrix can be written as

$$S(\phi) = \frac{1}{2} (s_1 e^{i\varphi_1} + s_2 e^{i\varphi_2}) \hat{I} + \frac{1}{2} (s_1 e^{i\varphi_1} - s_2 e^{i\varphi_2}) \times (e^{-i2\phi} \hat{\sigma}_+ + e^{i2\phi} \hat{\sigma}_-), \quad (7)$$

where \hat{I} is the identity matrix. Under the illumination of circularly polarized light $|\pm\rangle$, one can see that, the first term of Eq. (7) indicates the helicity unconverted part; while the second term indicates the helicity converted part that introduces an addition phase delay $\pm 2\phi$ for states $|\pm\rangle$, which is caused by the non-commutations between $e^{i\phi\sigma_3}$ and $\hat{\sigma}_\pm$. This additional phase is exactly the geometric P-B phase, which is equal to the area

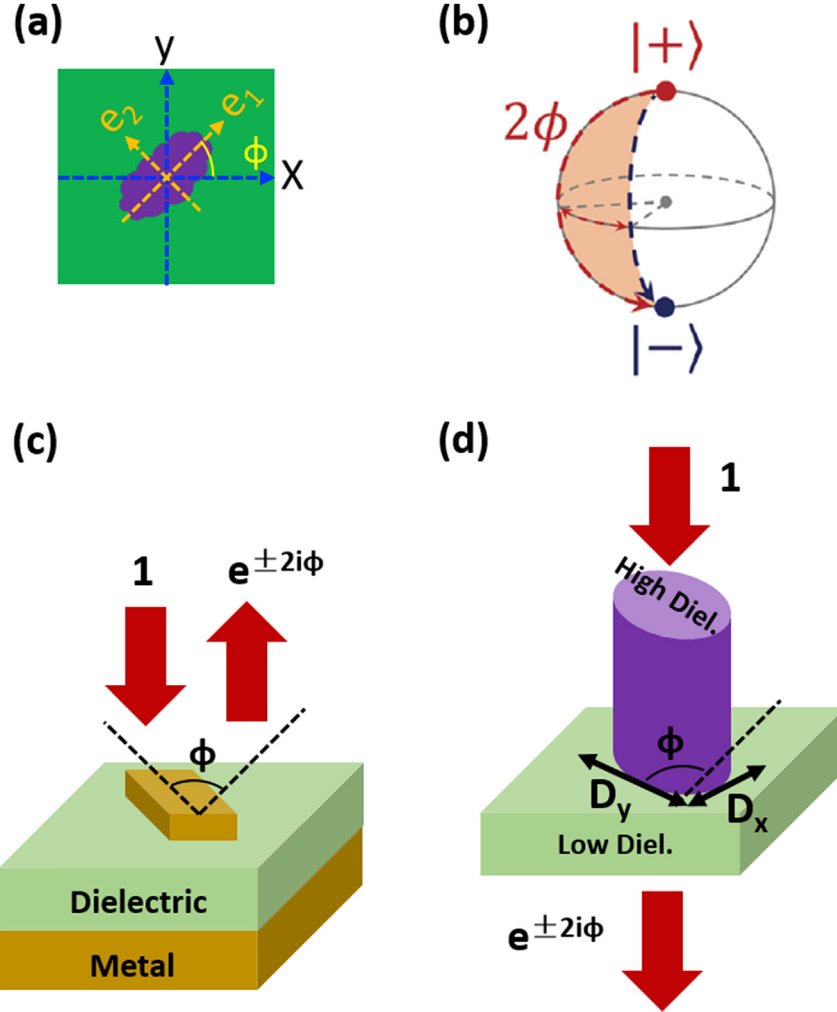


Fig. 3. The physical mechanism of geometric phase. (a) Schematic of an arbitrary anisotropic meta-atom with local frame (e_1, e_2) rotated by an angle ϕ with respect to the global frame (x, y). (b) The Poincaré sphere that illustrates origin of the geometric P-B phase, which is equal to the area surrounded by two curves with blue and red dashed lines. (c) The near-unity geometric phase modulation of reflected light from the metal-dielectric-metal meta-atom. (d) The near-unity geometric phase modulation of transmitted light from the high-index dielectric meta-atom.

surrounded by the closed loop created by two operations $\hat{\sigma}_\pm$ and $e^{-i\phi\sigma_3}\hat{\sigma}_\pm e^{i\phi\sigma_3}$ on $| \mp \rangle$ on the Poincaré's sphere shown in Fig. 3(b).

According to Eq. (7), the near-unity scattering efficiency of the geometric phase metasurface can be obtained if the first term of Eq. (7) vanishes, i.e. $s_1 e^{i\varphi_1} + s_2 e^{i\varphi_2} = 0$. This condition yields that:

$$s_1 = s_2, \quad \varphi_1 - \varphi_2 = 2n\pi + \pi, \quad (n \in \mathbb{Z}). \quad (8)$$

It indicates that, the anisotropic meta-atom should behave as a half-wave plate. There are two methods to design the high-efficient P-B type meta-atoms for reflection mode and transmission mode applications. The first approach uses the reflection-type metal-dielectric-metal structure (Fig. 3(c)). The high conversion efficiency between the two circular polarization states arises from the interplay of the localized plasmon resonance and the Fabry-Pérot effect on the tri-layer metasurface [47]. The second approach utilizes all-dielectric meta-atom working in transmission mode (Fig. 3(d)). The meta-atoms could be elliptical posts [53] or rectangular posts [14], whose short axis D_x and long axis D_y are manipulated to tailor the phases φ_1 and φ_2 of transmitted light wave, respectively. When the phase difference satisfies $\varphi_1 - \varphi_2 = \pi$, the near-unity efficiency can be obtained in the transmission-type metasurfaces. Note that, φ_1 and φ_2 from the meta-atom in Fig. 3(d) are referred to as

propagation phases. The propagation phase comes from the waveguide effect and can be independently tailored for specific holographic applications [53]. Once the propagation phase is combined with the geometry P-B phase, we can obtain metasurface holograms with much more functionalities than conventional ones [57].

2.2.1.3. Huygens phase based on overlapped double resonance. In the transmission-type plasmonic metasurfaces, the optical efficiency is usually very low due to the limited cross-polarization conversion efficiency and strong optical losses. To circumvent this constraint, Huygens metasurfaces based on overlapped electric and magnetic double resonances were proposed and first realized at microwave frequencies [81,82]. Recently, all-dielectric metasurfaces composed of high refractive index meta-atoms also receive more attentions in recent years due to their negligible losses in optical frequencies [83–86]. By tuning the diameter and height of the all-dielectric meta-atom, the electric dipole and magnetic dipole can overlap with each other with the same resonant strength and damping rate [83,84], which fulfills the Huygens condition [85,87,88]. In this way, one can design the highly efficient metasurfaces with desired phase modulations by varying either the

diameter of the silicon nanoresonator (Fig. 1e) [85,86], or the periodicity of the metasurface [10,89].

2.2.1.4. Propagation phase based on all-dielectric high aspect-ratio post. Moreover, dielectric metasurfaces with high aspect ratio dielectric meta-atoms attract much attentions due to their high optical efficiency in transmission mode [16,53,57,90–99]. The modulated phases on those metasurfaces originate from the propagation of the waveguide modes existing in the tall nanoposts. Different sizes of the nanoposts have different effective propagation constant, and thus different phase delay of the transmitted light. Therefore, the phase modulation of the metasurface can be realized by changing the diameter of the silicon nanoposts as shown in Fig. 1f, and the resonant mode (sharp dip in Fig. 1f) of the nanoposts should be avoided to improve the transmission efficiency. Compared with the Huygens all-dielectric meta-atoms, propagation phase based all-dielectric meta-atoms need much larger thickness with wavelength scale, which increases the fabrication challenges, while on the other hand, propagation phased meta-atoms provide more degrees of freedom with complete phase and polarization control [53].

In addition to the above phase modulation methods using metasurfaces with subwavelength size, there are other types of phases which have been also used for metasurface holography, such as the binary detour phase [54,56,100,101], holographic interferogram phase [38,102–106], photon sieve-based phase [107,108] and so on.

2.2.2. Metasurface hologram design algorithms

Box 3. Procedures to compute the metasurface holograms.

Firstly, the amplitude and phase profile of a CGH should be calculated. For a given 2D image shown in Fig. 4(a), the relation between the complex amplitude at the image plane $I(x_i, y_i)$ and that at the hologram plane $H(x_h, y_h)$ can be described by the general diffraction formula from the Huygens-Fresnel principle [32],

$$H(x_h, y_h) = \frac{1}{j\lambda} \iint I(x_i, y_i) K(\theta) \frac{\exp(ikr)}{r} dx_i dy_i, \quad (9)$$

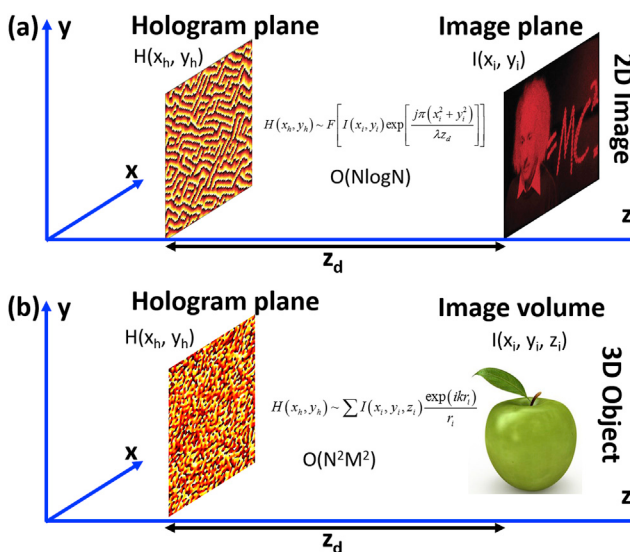


Fig. 4. Illustrations of the procedure to compute the phase profile of a meta-hologram. (a) The algorithm to compute the hologram of a 2D image can be reduced to the Fourier transform of a 2D matrix, which can be accelerated by FFT with computation complexity $O(N \log N)$. (b) The hologram of an arbitrary 3D object can be calculated by dividing the 3D object to a set of points or polygons. The computation complexity is $O(N^2 M^2)$.

where (x_h, y_h) and (x_i, y_i) are the coordinate frames of hologram and image planes, respectively, λ is the wavelength of light, $r = \sqrt{(x_h - x_i)^2 + (y_h - y_i)^2 + z_d^2}$, and $K(\theta)$ is an obliquity factor. In a practical computation, the uncertainty of $K(\theta)$ and the time-consuming integration operations for Eq. (9) make it difficult for programming implementations. Therefore, proper approximation should be applied to the practical computation procedure. When the distance between the hologram and image z_d is much larger than the feature sizes of both the hologram and image, we can utilize the paraxial approximation and simplify Eq. (9) as a Fresnel formula,

$$\begin{aligned} H(x_h, y_h) &= \frac{\exp(j2\pi z_d/\lambda)}{j\lambda z_d} \exp\left[\frac{j\pi(x_h^2 + y_h^2)}{\lambda z_d}\right] \\ &\cdot \iint I(x_i, y_i) \exp\left[\frac{j\pi(x_i^2 + y_i^2)}{\lambda z_d}\right] \exp\left[-j\frac{2\pi}{\lambda z_d}(x_h x_i + y_h y_i)\right] dx_i dy_i \\ &\frac{\exp(j2\pi z_d/\lambda)}{j\lambda z_d} \exp\left[\frac{j\pi(x_h^2 + y_h^2)}{\lambda z_d}\right] F\left[I(x_i, y_i) \exp\left[\frac{j\pi(x_i^2 + y_i^2)}{\lambda z_d}\right]\right], \end{aligned} \quad (10)$$

where, $F[\cdot]$ stands for the Fourier transformation (FT) evaluated using the spatial frequencies $(x_h/\lambda z_d, y_h/\lambda z_d)$. The FT computation can be implemented by the widely used Fast Fourier transform (FFT) algorithm without any integration computations. Assuming the pixel number in both the image plane and hologram plane is $N \times N$, the computation complexity of FFT is $O(N \log N)$, which is significantly reduced compared with the direct integration method with $O(N^4)$.

If z_d is even longer such that $z_d \gg \frac{\pi}{\lambda} (x_i^2 + y_i^2)_{\max}$, the hologram can be calculated by using the Fraunhofer diffraction formula,

$$\begin{aligned} H(x_h, y_h) &= \frac{\exp(j2\pi z_d/\lambda)}{j\lambda z_d} \exp\left[\frac{j\pi(x_h^2 + y_h^2)}{\lambda z_d}\right] \\ &\cdot \iint I(x_i, y_i) \exp\left[-j\frac{2\pi}{\lambda z_d}(x_h x_i + y_h y_i)\right] dx_i dy_i \\ &= \frac{\exp(j2\pi z_d/\lambda)}{j\lambda z_d} \exp\left[\frac{j\pi(x_h^2 + y_h^2)}{\lambda z_d}\right] F[I(x_i, y_i)], \end{aligned} \quad (11)$$

One can see that, the hologram profile is the FT of the image profile multiplied by a quadratic phase factor, with the same computation complexity $O(N \log N)$ of the Fresnel diffraction formula. However, the approximation condition for Fraunhofer diffraction is very stringent i. e. z_d should be deemed as an infinite value. Thus, in the practical experiment, a lens should be placed between the hologram plane and the image plane to reconstruct the holographic image.

To obtain the corresponding phase-only profile from an arbitrary wavefront with both amplitude and phase distribution, a random phase diffusers need to be added into the image plane, in combination with iterative FFT algorithm to homogenize the amplitude distribution at the hologram plane. Details of the iterative algorithm have been described in Gerchberg and Saxton's papers [34]. Then the calculated phase profile can be recorded by the meta-atoms with the phase modulation rules as we discussed in section 2.2.1.

The computation of CGH of a 3D object is more difficult than for the 2D case. At first, a 3D object needs to be discretized into a sets of points or polygons. The complex amplitude at each point (x_h, y_h) at the hologram plane can be calculated by superposition of the

contributions from all the constituent points or polygons of the 3D object,

$$H(x_h, y_h) = \frac{1}{J\lambda} \sum I(x_i, y_i, z_i) \frac{\exp(ikr_i)}{r_i}. \quad (12)$$

Assuming the number of points or polygons is M in each dimension, the computation complexity is $O(N^2M^2)$, which is much larger than that in the 2D case. To accelerate the computation of the hologram for a 3D object, the replacement of the summation or integration operations by FT operations in certain extends are considered [36,109].

2.2.3. Holographic images by meta-holograms with various types of meta-atoms

With the pre-defined phase distribution of the hologram calculated based on CGH algorithms [30,31], the metasurface is then fabricated according to the correspondence between the geometric parameter of meta-atom and the modulated phase. At visible-near infrared frequencies, the fabrication of photonic metasurface relies on the state of the art nano-fabrication techniques, such as electron-beam lithography, focused-ion beam milling, and so on. The first experimental demonstration of metasurface hologram are realized by using V-shaped (Fig. 5a) [110] and geometric P-B phase meta-atoms (Fig. 5b) [111]. In both cases, a single layer of gold meta-atom with ultrathin thickness (30 nm and 40 nm) and sub-wavelength pixel size (150 nm and 800 nm) was employed to construct the meta-hologram. Such compact feature size of the device makes the miniaturization and integration of multiple optical functionalities very convenient, which is difficult for conventional CGHs and the bulk metamaterial holograms [45,46]. However, for single layer plasmonic metasurfaces, the optical diffraction efficiencies are usually very low (<10%), due to the limited cross polarization conversion and optical losses in metal. To improve the optical diffraction efficiency of the meta-hologram, a metallic mirror and a dielectric spacer is placed under the geometric meta-atoms to form the F-P cavity and recycle the energy of incident light (Fig. 5c). The geometric parameters of dielectric spacer, meta-atoms can be optimized so that each meta-atom acts as a half-wave plate. The conversion efficiency between the incident Left (Right) circularly polarized (LCP/RCP) light into RCP/LCP light on the tri-layer meta-hologram is above 80%. Such high diffraction efficiency is only limited by the intrinsic ohmic loss of metal. Alternatively, high optical diffraction efficiency holography can be realized by employing lossless all-dielectric metasurfaces (Fig. 5d–f). From Fig. 5d, it is shown that the transmission efficiency of the Huygens-type silicon metasurface reaches near-unity and a phase modulation range of 0–2π was realized by tuning the lattice periodicity. Based on this scheme, high efficiency holographic image, a “hv” pattern was demonstrated [89]. Fig. 5e shows another Huygens-type dielectric metasurface holograms in which the phase modulation arises from various diameters of the silicon disks. In this work, near-unity transmission efficiency of ~0.9 was demonstrated for a broadband range from 1400 nm to 1650 nm [86]. In addition to the Huygens-type design, all-dielectric metasurfaces based on binary detour phase (Fig. 5f) [56] and propagation phase were also reported [53].

3. Polarization multiplexed metasurface hologram

Polarization multiplexing in optical holography plays an important role in various fields including information encryption, watermarking, and multifunctional diffractive optical elements. In earlier works on optical holography, polarization-dependent holographic multiplexing has been proposed in natural photo-induced anisotropic materials, which are typically realized by

Azobenzene materials [112]. Both the intensity and polarization of an object wave can be optically recorded by the photo-induced birefringence materials [113,114]. By setting two object waves with orthogonal polarizations, dual holographic images can be recorded in a single hologram [115]. However, such a way for polarization multiplexing can only be done by optical recording method, while it is not applicable for a CGH.

By fully exploiting the optical anisotropy of the meta-atom, polarization-dependent multiple holographic images can be easily encoded onto the metasurface. In principle, arbitrary polarization states including linear, elliptical and circular polarization states, can be used to realize information multiplexing on the metasurface platform.

3.1. Linear polarization multiplexed meta-holograms

The most straightforward way of polarization-multiplexing is to exploiting the anisotropy of meta-atoms. For example, two perpendicular anisotropic meta-atoms have independently response to two orthogonal linear polarizations of the incident light, respectively (Fig. 6). By encoding two sets of phase distributions independently into the two sets of meta-atoms, linear polarization multiplexed dual images can be constructed. This kind of anisotropic meta-atoms can be made by crossed or perpendicular plasmonic nanorods (Fig. 6a and b). Usually, very limited phase levels (4 levels for Fig. 6a and 2 levels for Fig. 6b) are adopted to encoding two holographic images. For vertical and horizontal polarized incident light, different images are readout, respectively. In Fig. 6c, perpendicular metallic nano-slits and detour phase are adopted for polarization multiplexing, different beam profiles (Airy beam in horizontal direction, and vortex beam in vertical direction) are generated by using reconstruction light beams with different polarizations. Fig. 6d shows the all-dielectric metasurfaces that can realize polarization multiplexing by using elliptical silicon meta-atoms. The long axis and short axis of the elliptical pillar can be independently tailored to modulate two sets of phase profile, and thus polarization-dependent dual images are encoded by a single subwavelength unit cell, which prevents the unwanted high-order diffractions.

3.2. Spin-dependent (circular polarization multiplexed) meta-holograms

The above mentioned hologram multiplexing schemes are based on but not limited to linear polarization of the incident light. Circular polarization state of light, which is associated with the spin angular momentum of photons, plays an important role in the emerging field of spin-orbit coupling of light [116–119]. Actually, the helicity of the circular polarization (or spin) of light can be also exploited to realize multiplexed dual holographic images. As shown in Fig. 7, spin-multiplexed metasurface holograms are mainly implemented by using the concept of geometric P-B phases. As shown in Fig. 7a, for incident light with LCP and RCP states, the position of the flower and bee images from the tri-layer metasurface will interchange with each other, exhibiting helicity-dependent behaviors. Based on the same procedure, helicity dependent multiple-functionalities with both holographic imaging and lensing capabilities are realized on one metasurface (Fig. 7b). By combining the geometric P-B phase and the detour phase (Fig. 7c), or by combining the geometric P-B phase with the waveguide propagation phase (Fig. 7d) together, spin dependent holographic multiplexing with much more functionalities can be realized. For example, arbitrarily orthogonal polarization (including linear, circular and elliptical polarizations) multiplexing schemes, can be obtained by using the combined geometric P-B phase and propagation phase [53,57].

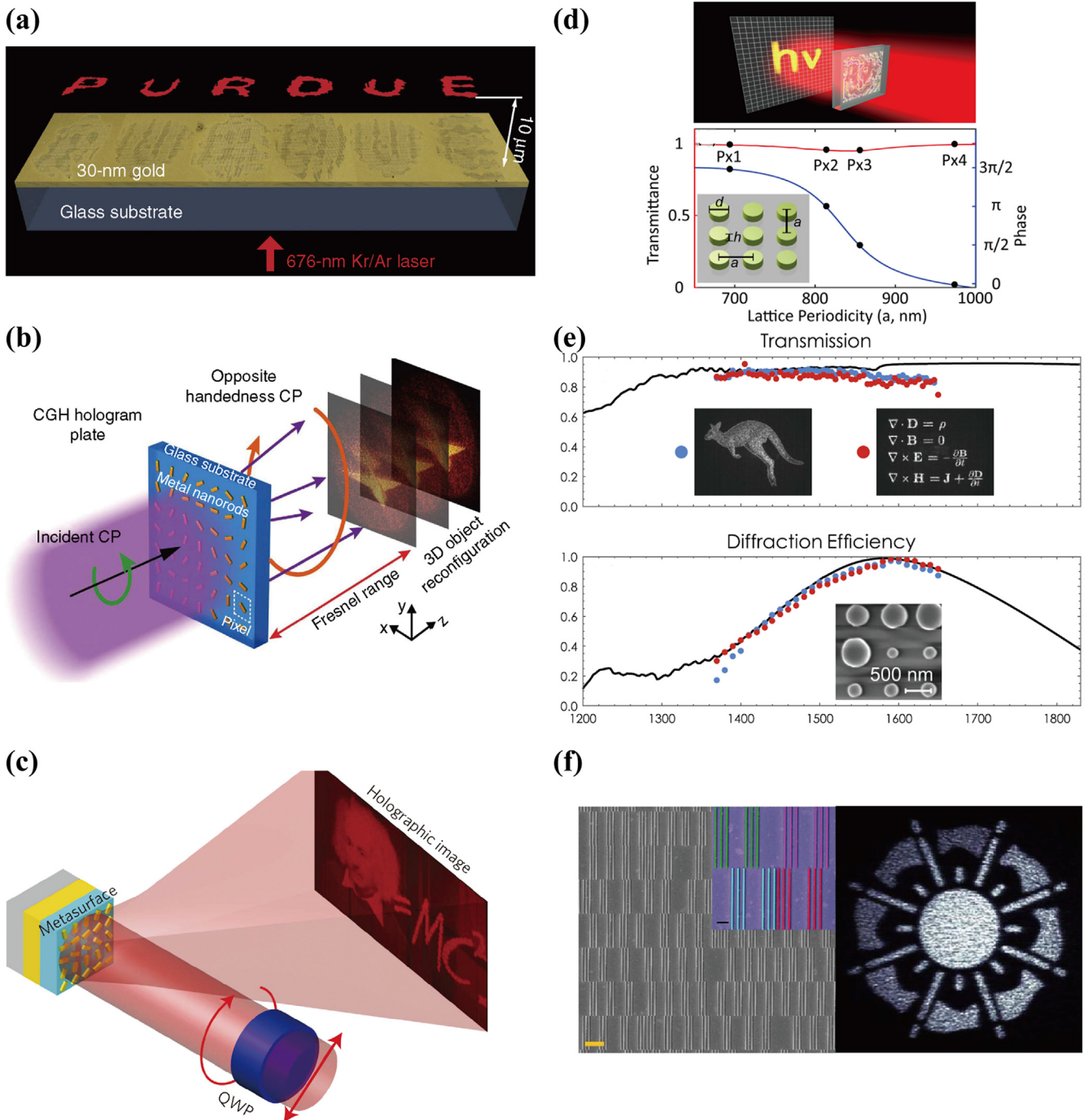


Fig. 5. Metasurface hologram realized by using different types of meta-atoms. (a) Holographic reconstructed letters with double resonant V-shaped meta-atoms [110]. (b) and (c) 3D holographic images reconstructed by using geometric P-B metasurface [111] and high efficiency tri-layer metasurface [47], respectively. (d) and (e) Holographic images reconstructed by using dielectric Huygens metasurfaces with high transmission efficiency [86,88,89]. (f) Holographic images reconstructed by using detour phase based metasurface hologram [56].

4. Wavelength multiplexed metasurface-holograms

The dimensionality of wavelength of light is also widely exploited to multiplex different holographic information. The concept of wavelength multiplexing on metasurfaces is especially useful in various aspects. For example, in the design of metasurface achromatic lens and super-dispersive optical diffraction elements, independent multiple phase profiles should be encoded at multiple wavelengths, in the purpose of compensating or enhancing the

dispersions [13,59,103,120–129]. By exploiting the integrated resonance effect of multiple meta-atoms, achromatic behavior can be obtained by in a continuous wavelength range [Fig. 8(a)] [18]; multiplexing different color information on different resonant unit cells can also lead to dynamic color displays [Fig. 8(b)] [130], selective color routings [131,132] and so on.

For metasurface holography, wavelength multiplexing is mainly applied to colorful 2D and 3D holographic imaging. It is known that high quality holographic imaging is always limited by tedious

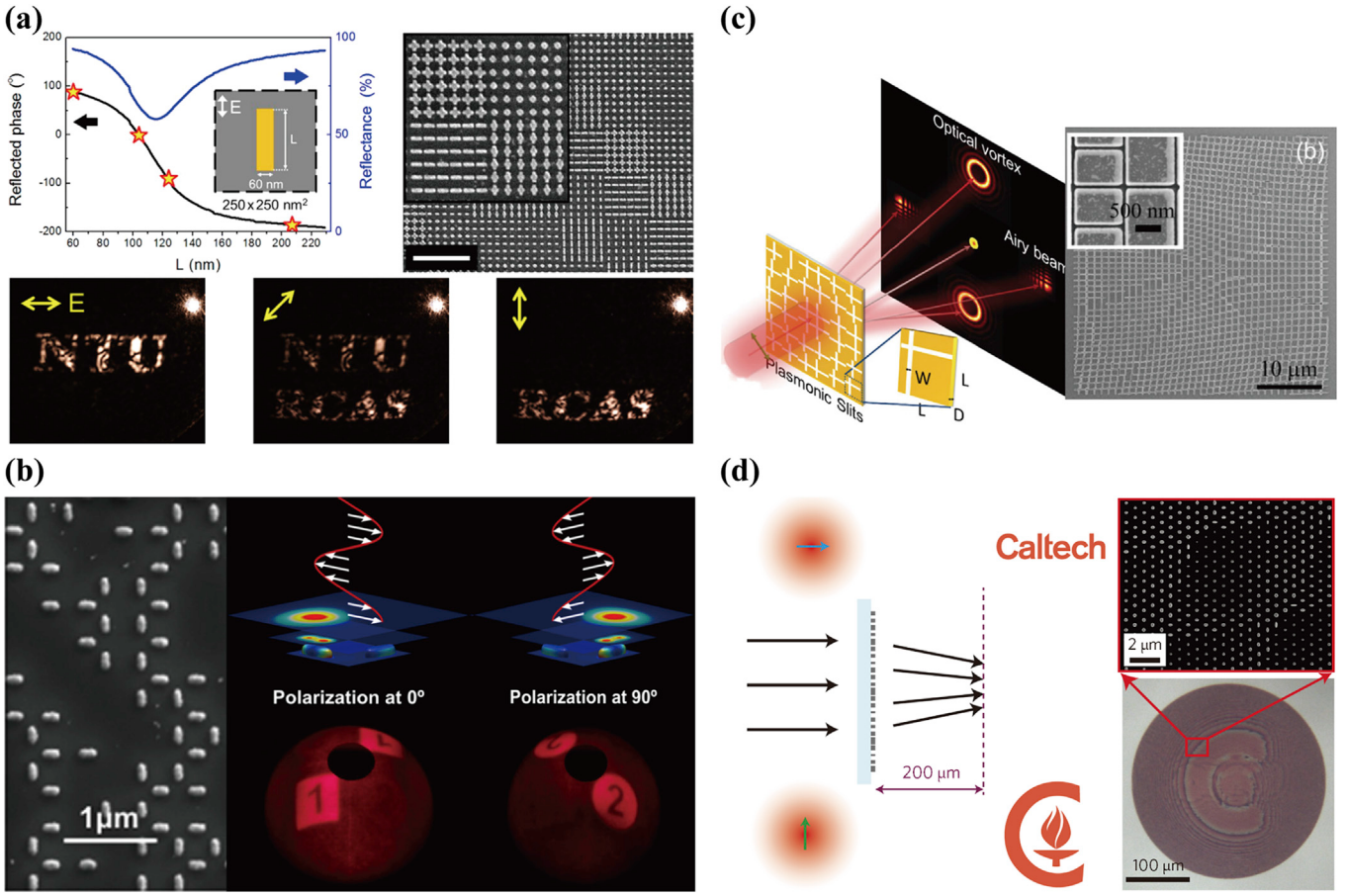


Fig. 6. Polarization multiplexed metasurface holograms. (a) Four phase levels [51] and (b) two phase levels metasurface holograms [52] realized by using perpendicular metallic nanorods. For horizontal and vertical polarized incident light, two different holographic images appear in the same imaging plane. (c) Perpendicular metallic slits based metasurface holograms that can reconstruct both vortex beam and Airy beam in different diffraction orders [54]. (d) Elliptical silicon posts that encode two independent phases with the long and short axis, respectively, leading to different images for different linear polarization states [53].

single color, therefore high performance colorful holography imaging is long-last pursued for practical applications. In conventional holography, colorful images can be obtained by the so called rainbow hologram [32,33]. However, it can only produce horizontal parallax, and the color of the image depends on the viewing angles in the vertical direction, which largely prevents its practical applications. Although colorful hologram can also be constructed using CGH and SLM [133–138], however, the technical difficulties such as poor imaging quality, limited color gamut, and narrow viewing angle have not been resolved. Metasurface holography, mediated by the resonance and dispersion of meta-atoms [37], provides a novel solution to produce high performance colorful holographic images. Here, we list two kinds of approaches to realize the wavelength multiplexed full-color holograms: 1. Multiplexing different holographic information with different sized meta-atoms, which response to different wavelengths [58,59,62,139], and then combining those multiple meta-atoms in a large unit cell; 2. Multiplexing different holographic information with the same kind of meta-atoms, while removing the crosstalk by shifting incident angles of the incident light with different wavelengths [49,50].

4.1. Multiplexing different holographic information with different sized meta-atoms

In Fig. 8c, three kinds of aluminum nanorods with resonant wavelengths of 405 nm, 532 nm and 658 nm are adopted for design

of metasurface. Because both the wavelength multiplexing and the phase modulation rely on the resonant feature of the nanorod meta-atoms, only two phase levels are modulated for the holographic imaging. All the red, green and blue colors are reconstructed in the holographic images which appear as “R”, “G”, and “B” letters, respectively. Due to the limited phase levels and the large pixel size of this kind of meta-hologram, multiple high-order images appears in the imaging plane. In Fig. 8d, three different sized silicon meta-atoms that support enhanced diffraction peaks at 473 nm, 532 nm and 633 nm, respectively, are utilized for a geometric metasurface. The phase modulation relies on the orientation of each meta-atoms, and therefore is independent of the wavelength. As a result, phase modulations with eight levels are realized to reconstruct the complex color images.

4.2. Multiplexing different holographic information with identical meta-atoms and different incident angles

Different from the previous approach that requires different kinds of meta-atoms and enlarged unit cell, the second wavelength-multiplexing approach requires only one type of meta-atom to generate the full-color holographic imaging, which prevents the unwanted high-order images and can extend the viewing angle of the metasurface. However, the wavelength multiplexed holographic information in this way should have some cross-talk effect. For example, under the red light illumination, the reconstructed image

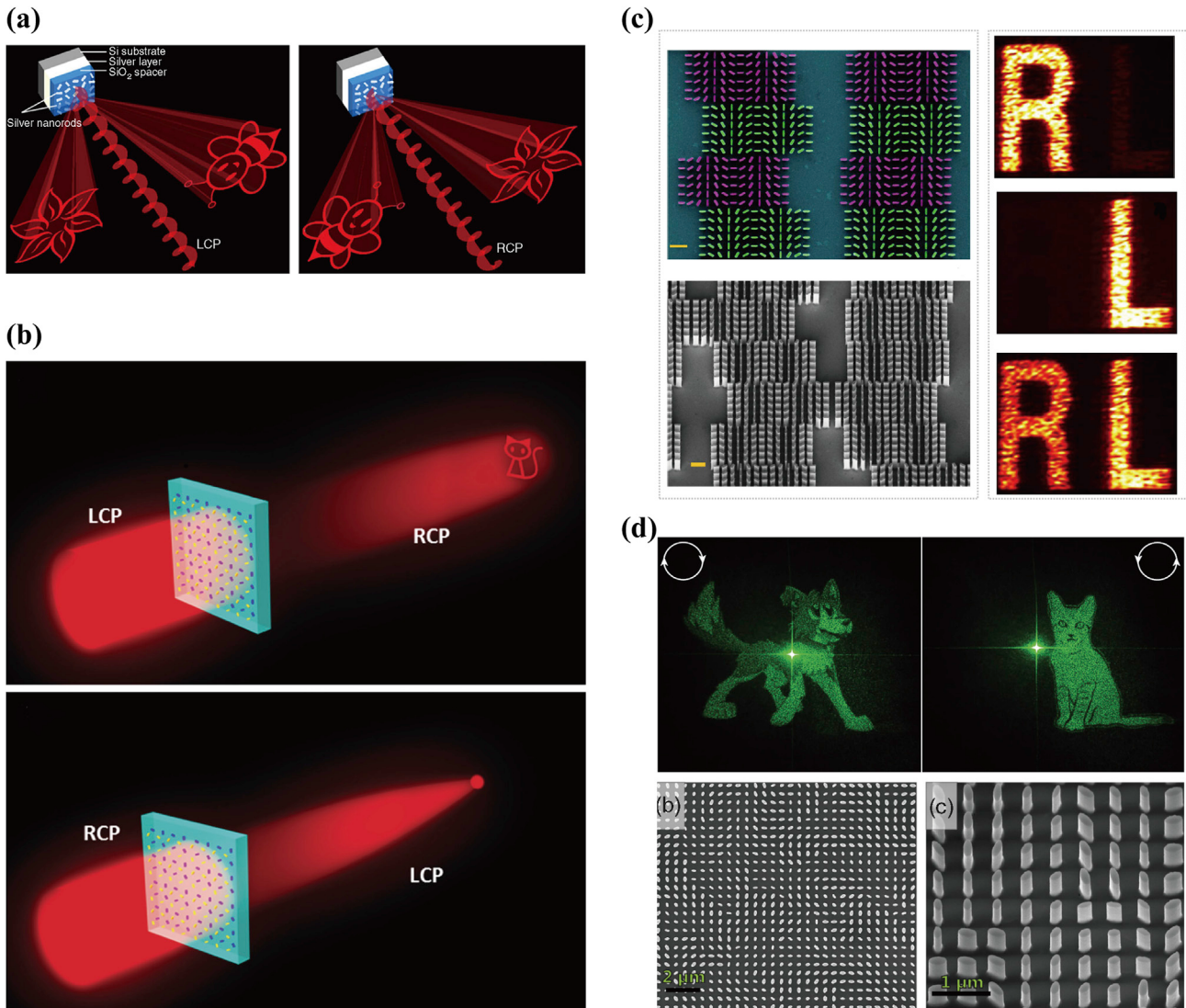


Fig. 7. Spin-dependent metasurface holograms. (a) Geometric P-B phase based metasurface holograms that can produce interchangeable dual images, by tuning the helicity of the incident circular polarizations [48]. (b) Geometric phase metasurfaces that demonstrate different functionalities, namely, holographic imaging and lensing, by tuning the circular polarization states of the incident light [55]. (c) Helicity-dependent binary metasurface holograms realized by silicon posts [56]. The holographic images of the RHC and LHC components are recorded by the green and purple silicon post arrays, respectively. (d) Elliptical TiO₂ meta-atoms that encode two independent holographic images by using the opposite helicities of the incident light [57].

contains not only the red patterns but also the unwanted image patterns designed for green and blue light. To shift the unwanted images of other wavelengths to different places, one can set different incident angles for different colored incident light (Fig. 9a). In this way, only the desired holographic images with different colors are present in the on-axis direction, while the other unwanted images are shifted to off-axis direction outside the observation zone. In Fig. 9(b), by arranging the incident light beams in a more complicated way so that the incident angles are varied in both the x and y directions, all the unwanted images can be converted into evanescent waves, which is totally out of the viewing field.

5. Other multiplexed metasurface holograms

5.1. Spatially-multiplexed metasurface holograms

There are also other ways to achieve multiplexed metasurface holograms. For example, by designing the metasurface with a phase profile obtained by superposition of the diffracted phase distributions

of multiple images placed at different spatial locations, spatially multiplexed meta-holograms can be constructed as shown in Fig. 10. Fig. 10a shows that for a metasurface hologram, four different 3D objects can be reconstructed at $z = -700\mu\text{m}$, $-500\mu\text{m}$, $500\mu\text{m}$, and $700\mu\text{m}$, respectively, with the field depth of $200\mu\text{m}$ between two adjacent images. As shown in Fig. 10b, an ultrathin gold metasurface consisting of pre-designed nano-slits can be used to generate spatially multiplexed optical vortex beams with different orbital angular momenta. Similarly, spatially multiplexed dielectric metasurface hologram was demonstrated in visible range (Fig. 10c). In addition, by placing the spatially multiplexed metasurface on a flexible substrate, different holographic images can be switched to each other by stretching or loosening the substrate (Fig. 10d).

5.2. Nonlinear photonic metasurface holograms

In the above metasurfaces, we only consider their linear optical properties. In fact, the nonlinear optical metasurface, which represents an emerging field in recent years [73,140], can also be

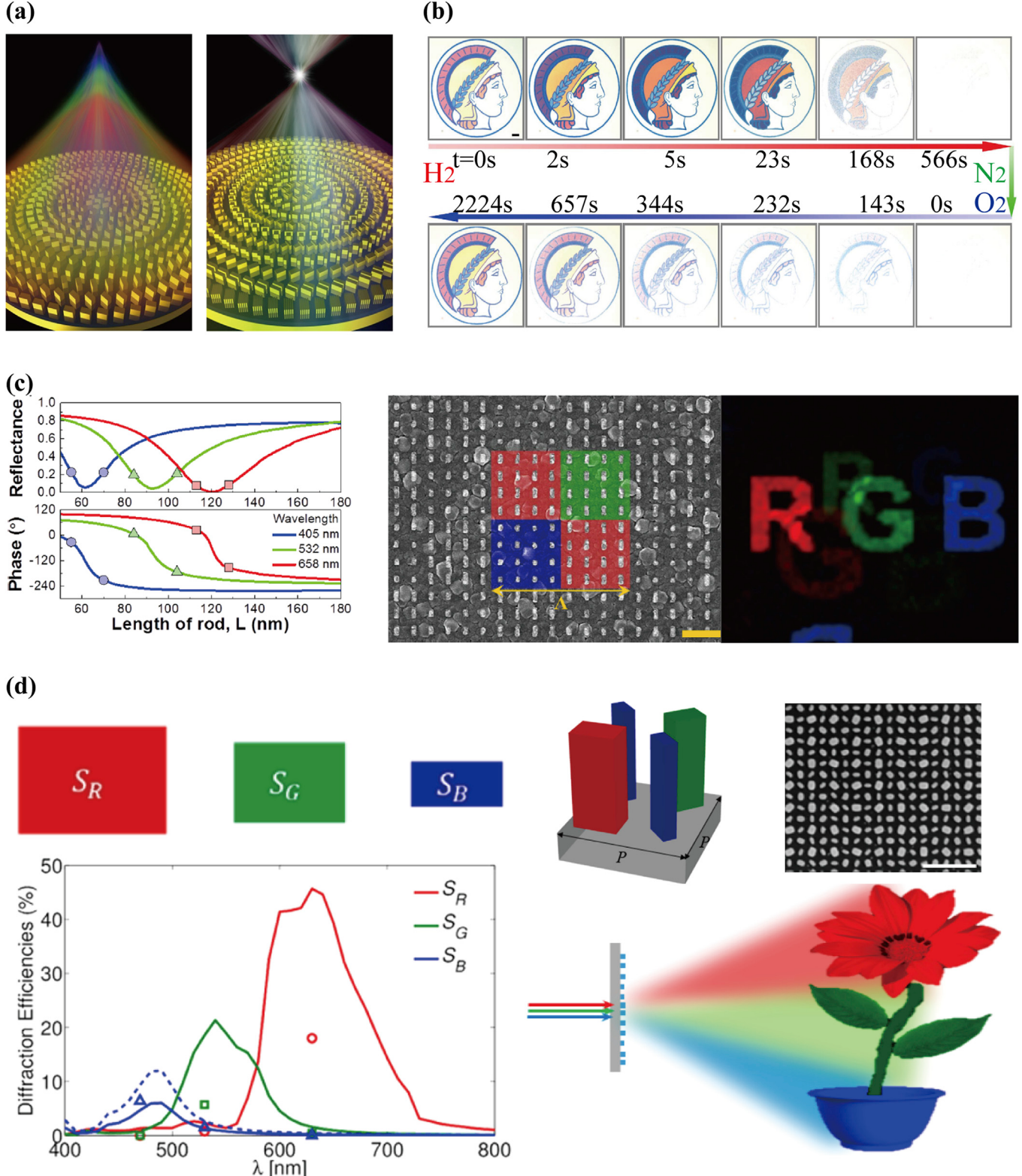
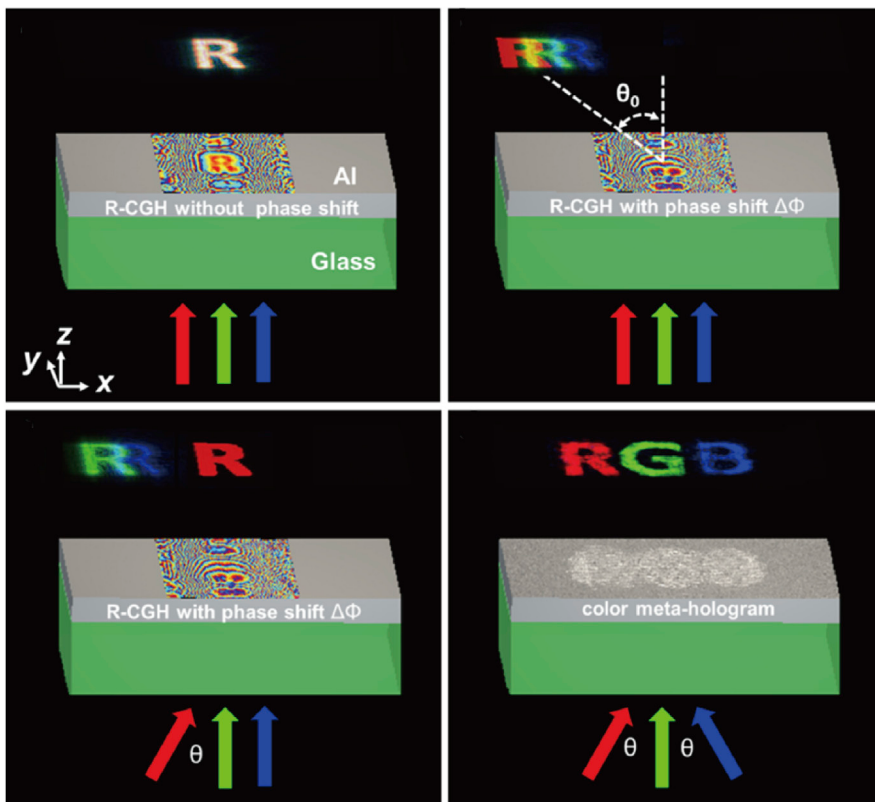


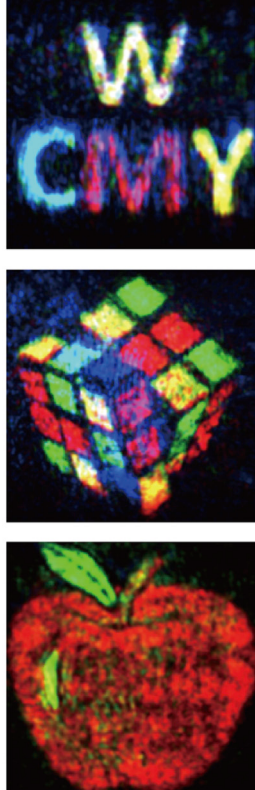
Fig. 8. Wavelength multiplexed metasurfaces by engineering the resonant properties of the meta-atoms. (a) Integrated resonances for continuous achromatic focusing [18], (b) plasmonic resonance engineered for dynamic color displaying [130]. (c) Holographic images with the primary three colors red, green and blue are designed by using Aluminum nanorods with resonant phase. In order to suppress the crosstalk between different colors, only two phase levels are modulated [58]. (d) Geometric phase metasurfaces constructed by using nanorods with both spatially varying orientations and sizes. The orientation modulates the phase profile of the hologram, while the size of the meta-atom determines the resonant frequencies, which are designed at the wavelengths of the three primary colors, leading to the final colorful holographic images [59].

(a)

Multiple-incident-beam configuration

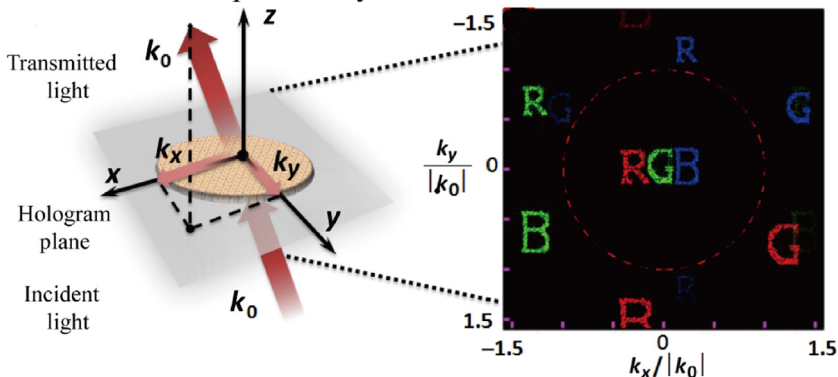


Reconstructed full-color images



(b)

k-space analysis of incident beams



Reconstructed multicolor image



Fig. 9. Wavelength multiplexed color metasurface holograms by shifting different incident angles for different light wavelengths. (a) Incident angles of multiple beams are varied in x direction [49]. (b) Incident angles of multiple beams are varied in both x and y directions, enabling the conversion of unwanted images into evanescent waves [50].

exploited to achieve multiplexed meta-holograms. In Fig. 11a, both the fundamental wave and the second harmonic generation (SHG) wave used to encode different holographic images. For an incident light with LCP polarization (spin σ), the fundamental wave with opposite helicity (RCP) has the geometric phase $2\sigma\varphi(\mathbf{r})$, where $\varphi(\mathbf{r})$ is the orientation angle of the meta-atom at position \mathbf{r} ; while the nonlinear wave from SHG of spin σ and spin $-\sigma$ have nonlinear geometric phase $\sigma\varphi(\mathbf{r})$ and $3\sigma\varphi(\mathbf{r})$, respectively. All the three phases were used to multiplex the letters "X", "R", "L", respectively. Moreover, by controlling the destructive and constructive interferences of the SHG waves from two neighboring meta-atoms

(Fig. 11b), predefined images can only be readout from the SHG probing wave. This kind of nonlinear metasurface technique can be used for information encryption, anticounterfeiting applications and so on.

6. Conclusions and perspective

We have overviewed the rapid development of metasurface holography and its various applications. From the perspectives of physical mechanism, the approaches of phase modulation, including the resonant phase, Geometric P-B phase, Huygens phase, and

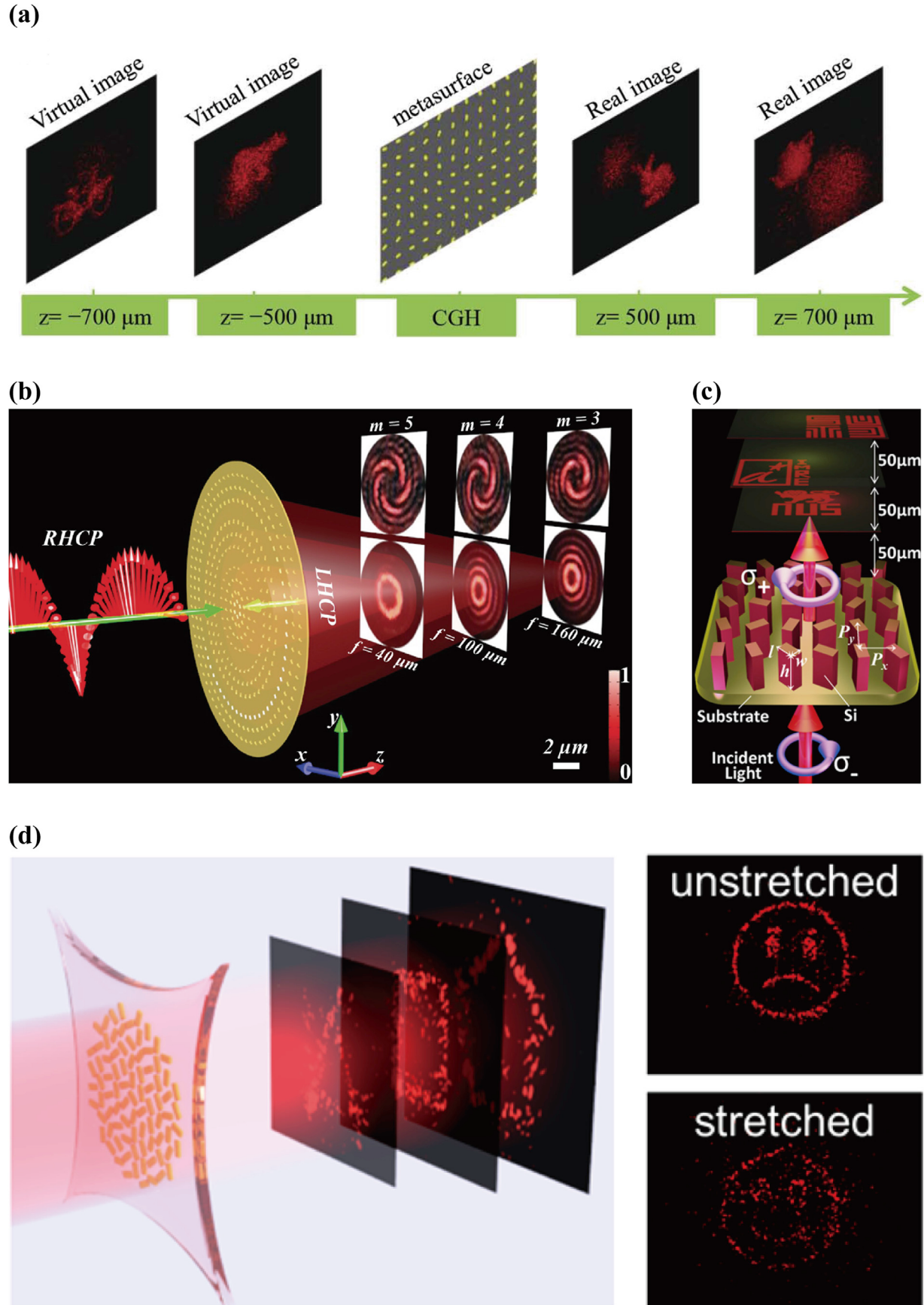


Fig. 10. Spatially multiplexed metasurface holograms. (a) four 3D holographic images are reconstructed at different z-axis positions [64]. (b) Vortex beams with different topological charges are generated at different places [65]. (c) Spatially multiplexed metasurface holograms at visible frequencies, realized by using an all-dielectric metasurface [66]. (d) Different holographic images appear in different places realized with a flexible metasurface, one can switch the appearance of different images by stretching the metasurface [67].

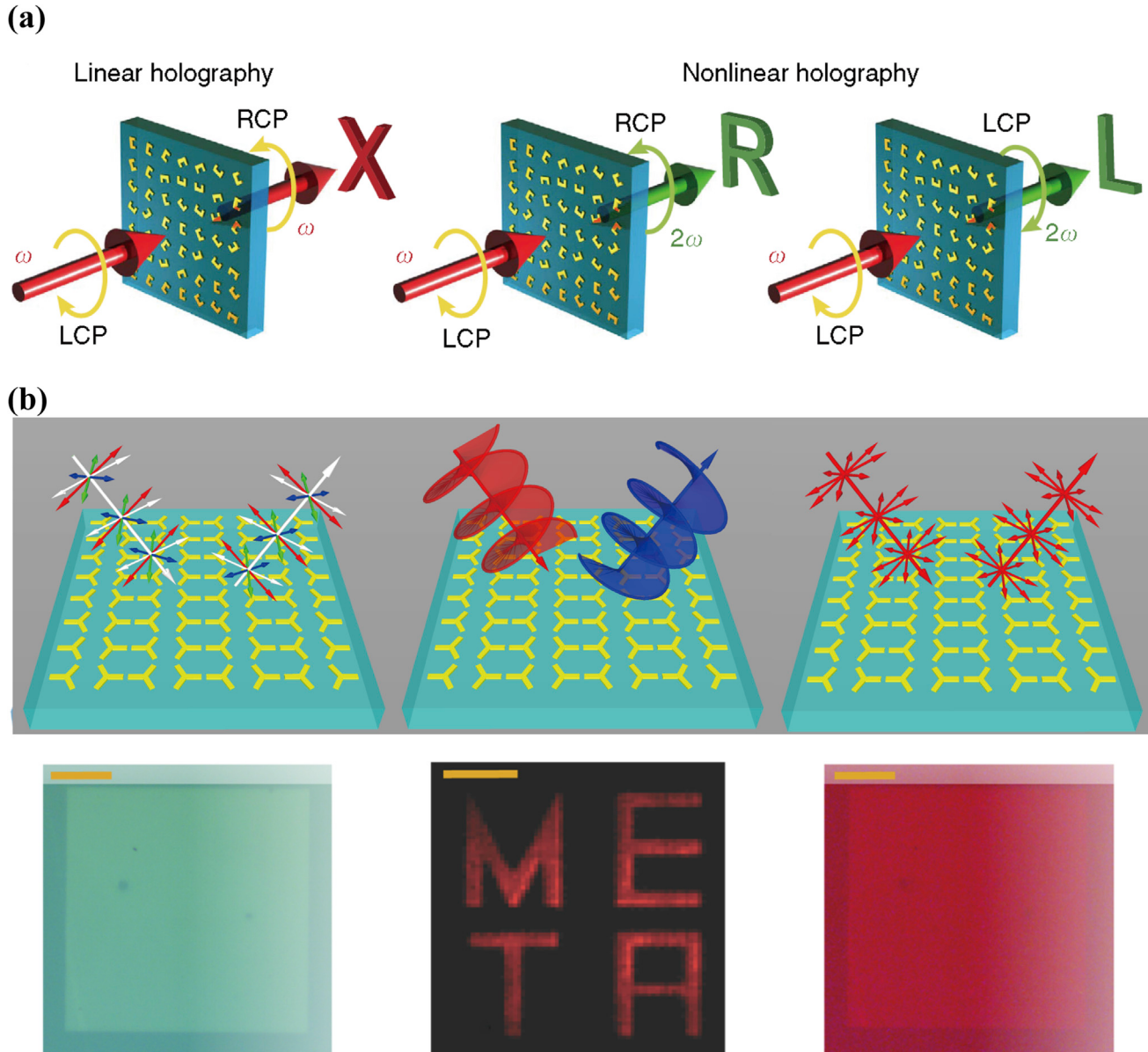


Fig. 11. Nonlinear photonic metasurface. (a) Both spin and wavelength multiplexed holograms which can encode multiple optical images at both the fundamental wavelength and the second harmonic generation wavelength [70]. (b) Optical information encryption based on the nonlinear photonic metasurface, adopted from Ref. [71].

propagation phase are summarized. Based on those phase modulation mechanisms, both 2D and 3D holographic images with large viewing angle, high diffraction efficiency, high image quality and full-color performances were demonstrated on the metasurface platform. After that, we review the efforts in information multiplexing using the degrees of freedom of polarization, wavelength and so on. For the polarization multiplexing technique, it is shown that both crossed linear and circular polarizations can be used to independently multiplex dual holographic images. Alternatively, one can multiplex wavelength dependent holographic information using either different types of meta-atoms that have different resonant wavelengths, or the same kind of meta-atoms with different incident angles. Moreover, multiplexing holographic information on metasurfaces can also be implemented by using degrees of freedom of spatial information and nonlinear optical processes.

Although many great progresses have been achieved in the field of metasurface holography, there are still exist some challenges to

be overcome in future. Nowadays, nanofabrication of the metasurface holograms mainly relies on high-cost and time-consuming electron beam lithography or focused ion beam etching, which may hinder the potential applications of metasurface optical devices. Nanoprinting should be a feasible way to the low cost and large area fabrication of photonic metasurfaces. On the other hand, one of the ultimate goals for metasurface holograms is the dynamic 2D or 3D holographic displaying for nowdays TV and smart phones. However, most of current metasurface holograms can only encode static images. In terahertz or microwave regime, graphene [141,142] and electrically tunable printed-circuit-board [143], Liquid-Metal [144] can be used to dynamically control the holographic images. At optical frequencies, the integration of phase change material [145–147], conducting oxide [148] can be used dynamically modulate the phase profile in a certain range, but still cannot meet the requirement for dynamic holographic display. Thus, novel optical materials and metasurface configurations through electro-

optic or all-optical control should be developed to realize the real-time dynamic holographic display.

Acknowledgements

G. X. was supported by Natural Science Foundation of Shenzhen Innovation Committee (Grant No. JCYJ20170412153113701) and the National Natural Science Foundation of China (Grant No. 11774145). Z. L. was supported by the National Natural Science Foundation of China (Grant No. 11604217) and the Fundamental Research Funds for the Central Universities (Grant No. 21617410).

References

- [1] C.M. Soukoulis, M. Wegener, Past achievements and future challenges in the development of three-dimensional photonic metamaterials, *Nat. Phot.* 5 (9) (2011) 523–530.
- [2] N. Yu, P. Genevet, M.A. Kats, F. Aieta, J.-P. Tetienne, F. Capasso, Z. Gaburro, Light propagation with phase discontinuities: generalized laws of reflection and refraction, *Science* 334 (6054) (2011) 333–337.
- [3] S. Sun, Q. He, S. Xiao, Q. Xu, X. Li, L. Zhou, Gradient-index meta-surfaces as a bridge linking propagating waves and surface waves, *Nat. Mater.* 11 (5) (2012) 426–431.
- [4] L. Huang, X. Chen, H. Mühlenernd, G. Li, B. Bai, Q. Tan, G. Jin, T. Zentgraf, S. Zhang, Dispersionless phase discontinuities for controlling light propagation, *Nano Lett.* 12 (11) (2012) 5750–5755.
- [5] F. Aieta, P. Genevet, N. Yu, M.A. Kats, Z. Gaburro, F. Capasso, Out-of-Plane reflection and refraction of light by anisotropic optical antenna metasurfaces with phase discontinuities, *Nano Lett.* 12 (3) (2012) 1702–1706.
- [6] Y. Yang, W. Wang, P. Moitra, I.I. Kravchenko, D.P. Briggs, J. Valentine, Dielectric meta-reflectarray for broadband linear polarization conversion and optical vortex generation, *Nano Lett.* 14 (3) (2014) 1394–1399.
- [7] S. Chen, Y. Cai, G. Li, S. Zhang, K.W. Cheah, Geometric metasurface fork gratings for vortex-beam generation and manipulation, *Laser Photonics Rev.* 10 (2) (2016) 322–326.
- [8] P. Genevet, N. Yu, F. Aieta, J. Lin, M.A. Kats, R. Blanchard, M.O. Scully, Z. Gaburro, F. Capasso, Ultra-thin plasmonic optical vortex plate based on phase discontinuities, *Appl. Phys. Lett.* 100 (1) (2012) 013101.
- [9] E. Karimi, S.A. Schulz, I. De Leon, H. Qassim, J. Upham, R.W. Boyd, Generating optical orbital angular momentum at visible wavelengths using a plasmonic metasurface, *Light Sci. Appl.* 3 (2014) e167.
- [10] K.E. Chong, I. Staudte, A. James, J. Dominguez, S. Liu, S. Campione, G.S. Subramania, T.S. Luk, M. Decker, D.N. Neshev, I. Brener, Y.S. Kivshar, Polarization-independent silicon metadevices for efficient optical wavefront control, *Nano Lett.* 15 (8) (2015) 5369–5374.
- [11] F. Aieta, P. Genevet, M.A. Kats, N. Yu, R. Blanchard, Z. Gaburro, F. Capasso, Aberration-free ultrathin flat lenses and axicons at telecom wavelengths based on plasmonic metasurfaces, *Nano Lett.* 12 (9) (2012) 4932–4936.
- [12] X. Chen, L. Huang, H. Mühlenernd, G. Li, B. Bai, Q. Tan, G. Jin, C.-W. Qiu, S. Zhang, T. Zentgraf, Dual-polarity plasmonic metalens for visible light, *Nat. Commun.* 3 (2012) 1198.
- [13] F. Aieta, M.A. Kats, P. Genevet, F. Capasso, Multiwavelength achromatic metasurfaces by dispersive phase compensation, *Science* 347 (6228) (2015) 1342–1345.
- [14] M. Khorasaninejad, W.T. Chen, R.C. Devlin, J. Oh, A.Y. Zhu, F. Capasso, Metalenses at visible wavelengths: diffraction-limited focusing and sub-wavelength resolution imaging, *Science* 352 (6290) (2016) 1190–1194.
- [15] M. Khorasaninejad, W.T. Chen, J. Oh, F. Capasso, Super-dispersive Off-Axis meta-lenses for compact high resolution spectroscopy, *Nano Lett.* 16 (6) (2016) 3732–3737.
- [16] M. Khorasaninejad, A.Y. Zhu, C. Roques-Carmes, W.T. Chen, J. Oh, I. Mishra, R.C. Devlin, F. Capasso, Polarization-Insensitive metalenses at visible wavelengths, *Nano Lett.* (2016).
- [17] G. Zheng, W. Wu, Z. Li, S. Zhang, M.Q. Mehmood, P.A. He, S. Li, Dual field-of-view step-zoom metalens, *Opt. Lett.* 42 (7) (2017) 1261–1264.
- [18] S. Wang, P.C. Wu, V.-C. Su, Y.-C. Lai, C. Hung Chu, J.-W. Chen, S.-H. Lu, J. Chen, B. Xu, C.-H. Kuan, T. Li, S. Zhu, D.P. Tsai, Broadband achromatic optical metasurface devices, *Nat. Comm.* 8 (1) (2017) 187.
- [19] Y. Zhao, A. Alù, Manipulating light polarization with ultrathin plasmonic metasurfaces, *Phys. Rev. B* 84 (20) (2011) 205428.
- [20] C. Pfeiffer, A. Grbic, Cascaded metasurfaces for complete phase and polarization control, *Appl. Phys. Lett.* 102 (23) (2013), 231116.
- [21] N. Yu, F. Aieta, P. Genevet, M.A. Kats, Z. Gaburro, F. Capasso, A broadband, background-free quarter-wave plate based on plasmonic metasurfaces, *Nano Lett.* 12 (12) (2012) 6328–6333.
- [22] P.C. Wu, W.-Y. Tsai, W.T. Chen, Y.-W. Huang, T.-Y. Chen, J.-W. Chen, C.Y. Liao, C.H. Chu, G. Sun, D.P. Tsai, Versatile polarization generation with an aluminum plasmonic metasurface, *Nano Lett.* 17 (1) (2017) 445–452.
- [23] T. Li, L. Huang, J. Liu, Y. Wang, T. Zentgraf, Tunable wave plate based on active plasmonic metasurfaces, *Opt. Express* 25 (4) (2017) 4216–4226.
- [24] A.V. Kildishev, A. Boltasseva, V.M. Shalaev, Planar photonics with metasurfaces, *Science* 339 (6125) (2013), 1232009.
- [25] N. Yu, F. Capasso, Flat optics with designer metasurfaces, *Nat. Mater.* 13 (2) (2014) 139–150.
- [26] N. Meinzer, W.L. Barnes, I.R. Hooper, Plasmonic meta-atoms and metasurfaces, *Nat. Phot.* 8 (12) (2014) 889–898.
- [27] P. Genevet, F. Capasso, F. Aieta, M. Khorasaninejad, R. Devlin, Recent advances in planar optics: from plasmonic to dielectric metasurfaces, *Optica* 4 (1) (2017) 139–152.
- [28] H.-T. Chen, J.T. Antoinette, N. Yu, A review of metasurfaces: physics and applications, *Rep. Prog. Phys.* 79 (7) (2016) 076401.
- [29] D. Gabor, A new microscopic principle, *Nature* 161 (1948) 777–778.
- [30] C. Slinger, C. Cameron, M. Stanley, Computer-generated holography as a generic display technology, *Computer* 38 (8) (2005) 46–53.
- [31] D.P. Kelly, D.S. Monaghan, N. Pandey, T. Kozacki, Micha, A. kiewicz, G. Finke, B.M. Hennelly, M. Kujawinska, Digital holographic capture and optoelectronic reconstruction for 3D displays, *Int. J. Digital Multimedia Broadcast*, 2010 (2010).
- [32] J.W. Goodman, *Introduction to fourier optics*, Roberts Co. (2004).
- [33] T.C. Poon, *Digital Holography and Three-dimensional Display*, Springer, 2006.
- [34] R.W. Gerchberg, W.O. Saxton, A practical algorithm for the determination of the phase from image and diffraction plane pictures, *Opt. (Jena)* 35 (1972) 237.
- [35] Y.-Z. Liu, X.-N. Pang, S. Jiang, J.-W. Dong, Viewing-angle enlargement in holographic augmented reality using time division and spatial tiling, *Opt. Express* 21 (10) (2013) 12068–12076.
- [36] Y.-Z. Liu, J.-W. Dong, Y.-Y. Pu, H.-X. He, B.-C. Chen, H.-Z. Wang, H. Zheng, Y. Yu, Fraunhofer computer-generated hologram for diffused 3D scene in Fresnel region, *Opt. Lett.* 36 (11) (2011) 2128–2130.
- [37] M. Ozaki, J.-i. Kato, S. Kawata, Surface-plasmon holography with white-light illumination, *Science* 332 (6026) (2011) 218–220.
- [38] I. Dolev, I. Epstein, A. Arie, Surface-plasmon holographic beam shaping, *Phys. Rev. Lett.* 109 (20) (2012) 203903.
- [39] C.M. Chang, M.L. Tseng, B.H. Cheng, C.H. Chu, Y.Z. Ho, H.W. Huang, Y.-C. Lan, D.-W. Huang, A.Q. Liu, D.P. Tsai, Three-dimensional plasmonic micro projector for light manipulation, *Adv. Mater* 25 (8) (2013) 1118–1123.
- [40] P. Genevet, F. Capasso, Holographic optical metasurfaces: a review of current progress, *Rep. Prog. Phys.* 78 (2) (2015) 024401.
- [41] Q. Xu, X. Zhang, Y. Xu, C. Ouyang, Z. Tian, J. Gu, J. Li, S. Zhang, J. Han, W. Zhang, Polarization-controlled surface plasmon holography, *Laser Photonics Rev.* (2016), 1600212-n/a.
- [42] J. Chen, T. Li, S. Wang, S. Zhu, Multiplexed holograms by surface plasmon propagation and polarized scattering, *Nano Lett.* (2017), <https://doi.org/10.1021/acs.nanolett.1027b02295>.
- [43] X. Li, H. Ren, X. Chen, J. Liu, Q. Li, C. Li, G. Xue, J. Jia, L. Cao, A. Sahu, B. Hu, Y. Wang, G. Jin, M. Gu, Athermally photoreduced graphene oxides for three-dimensional holographic images, *Nat. Comm.* 6 (2015) 6984.
- [44] Z. Yue, G. Xue, J. Liu, Y. Wang, M. Gu, Nanometric holograms based on a topological insulator material 8 (2017) 15354.
- [45] S. Larouche, Y.-J. Tsai, T. Tyler, N.M. Jokerst, D.R. Smith, Infrared metamaterial phase holograms, *Nat. Mater.* 11 (5) (2012) 450–454.
- [46] B. Walther, C. Helgert, C. Rockstuhl, F. Setzpfandt, F. Eilenberger, E.-B. Kley, F. Lederer, A. Tünemann, T. Pertsch, Spatial and spectral light shaping with metamaterials, *Adv. Mater* 24 (47) (2012) 6300–6304.
- [47] G. Zheng, H. Mühlenernd, M. Kenney, G. Li, T. Zentgraf, S. Zhang, Metasurface holograms reaching 80% efficiency, *Nat. Nano* 10 (4) (2015) 308–312.
- [48] D. Wen, F. Yue, G. Li, G. Zheng, K. Chan, S. Chen, M. Chen, K.F. Li, P.W.H. Wong, K.W. Cheah, E. Yue Bun Pun, S. Zhang, X. Chen, Helicity multiplexed broadband metasurface holograms, *Nat. Commun.* 6 (2015) 8241.
- [49] W. Wan, J. Gao, X. Yang, Full-color plasmonic metasurface holograms, *ACS Nano* 10 (12) (2016) 10671–10680.
- [50] X. Li, L. Chen, Y. Li, X. Zhang, M. Pu, Z. Zhao, X. Ma, Y. Wang, M. Hong, X. Luo, Multicolor 3D meta-holography by broadband plasmonic modulation, *Sci. Adv.* 2 (11) (2016), <https://doi.org/10.1126/sciadv.1601102>.
- [51] W.T. Chen, K.-Y. Yang, C.-M. Wang, Y.-W. Huang, G. Sun, I.D. Chiang, C.Y. Liao, W.-L. Hsu, H.T. Lin, S. Sun, L. Zhou, A.Q. Liu, D.P. Tsai, High-efficiency broadband meta-hologram with polarization-controlled dual images, *Nano Lett.* 14 (1) (2013) 225–230.
- [52] Y. Montelongo, J.O. Tenorio-Pearl, W.I. Milne, T.D. Wilkinson, Polarization switchable diffraction based on subwavelength plasmonic nanoantennas, *Nano Lett.* 14 (1) (2014) 294–298.
- [53] A. Arbabi, Y. Horie, M. Bagheri, A. Faraon, Dielectric metasurfaces for complete control of phase and polarization with subwavelength spatial resolution and high transmission, *Nat. Nano* 10 (11) (2015) 937–943.
- [54] C. Min, J. Liu, T. Lei, G. Si, Z. Xie, J. Lin, L. Du, X. Yuan, Plasmonic nano-slits assisted polarization selective detour phase meta-hologram, *Laser Photonics Rev.* 10 (6) (2016) 978–985.
- [55] D. Wen, S. Chen, F. Yue, K. Chan, M. Chen, M. Ardon, K.F. Li, P.W.H. Wong, K.W. Cheah, E.Y.B. Pun, G. Li, S. Zhang, X. Chen, Metasurface device with helicity-dependent functionality, *Adv. Opt. Mater* 4 (2) (2016) 321–327.
- [56] M. Khorasaninejad, A. Ambrosio, P. Kanhaiya, F. Capasso, Broadband and chiral binary dielectric meta-holograms, *Sci. Adv.* 2 (5) (2016), <https://doi.org/10.1126/sciadv.1501258>.
- [57] J.P. Balthasar Mueller, N.A. Rubin, R.C. Devlin, B. Groever, F. Capasso,

- Metasurface polarization optics: independent phase control of arbitrary orthogonal states of polarization, *Phys. Rev. Lett.* 118 (11) (2017) 113901.
- [58] Y.-W. Huang, W.T. Chen, W.-Y. Tsai, P.C. Wu, C.-M. Wang, G. Sun, D.P. Tsai, Aluminum plasmonic multicolor meta-hologram, *Nano Lett.* 15 (5) (2015) 3122–3127.
- [59] B. Wang, F. Dong, Q.-T. Li, D. Yang, C. Sun, J. Chen, Z. Song, L. Xu, W. Chu, Y.-F. Xiao, Q. Gong, Y. Li, Visible-frequency dielectric metasurfaces for multi-wavelength achromatic and highly dispersive holograms, *Nano Lett.* 16 (8) (2016) 5235–5240.
- [60] Y. Montelongo, J.O. Tenorio-Pearl, C. Williams, S. Zhang, W.I. Milne, T.D. Wilkinson, Plasmonic nanoparticle scattering for color holograms, *PNAS* 111 (35) (2014) 12679–12683.
- [61] A. Chanaia, A. Paulsen, S. Guruswamy, A. Nahata, Hiding multi-level multi-color images in terahertz metasurfaces, *Optica* 3 (12) (2016) 1466–1470.
- [62] W. Zhao, B. Liu, H. Jiang, J. Song, Y. Pei, Y. Jiang, Full-color hologram using spatial multiplexing of dielectric metasurface, *Opt. Lett.* 41 (1) (2016) 147–150.
- [63] B. Wang, B. Quan, J. He, Z. Xie, X. Wang, J. Li, Q. Kan, Y. Zhang, Wavelength de-multiplexing metasurface hologram, *Sci. Rep.* 6 (2016) 35657.
- [64] L. Huang, H. Mühlenbernd, X. Li, X. Song, B. Bai, Y. Wang, T. Zentgraf, Broadband hybrid holographic multiplexing with geometric metasurfaces, *Adv. Mater* 27 (41) (2015) 6444–6449.
- [65] M.Q. Mahmood, S. Mei, S. Hussain, K. Huang, S.Y. Siew, L. Zhang, T. Zhang, X. Ling, H. Liu, J. Teng, A. Danner, S. Zhang, C.-W. Qiu, Visible-frequency metasurface for structuring and spatially multiplexing optical vortices, *Adv. Mater* 28 (13) (2016) 2533–2539.
- [66] K. Huang, Z. Dong, S. Mei, L. Zhang, Y. Liu, H. Liu, H. Zhu, J. Teng, B. Luk'yanchuk, J.K.W. Yang, C.-W. Qiu, Silicon multi-meta-holograms for the broadband visible light, *Laser Photonics Rev.* 10 (3) (2016) 500–509.
- [67] S.C. Malek, H.-S. Ee, R. Agarwal, Strain multiplexed metasurface holograms on a stretchable substrate, *Nano Lett.* 17 (6) (2017) 3641–3645.
- [68] M. Tymchenko, J.S. Gomez-Diaz, J. Lee, N. Nookala, M.A. Belkin, A. Alù, Gradient nonlinear pancharatnam-berry metasurfaces, *Phys. Rev. Lett.* 115 (20) (2015) 207403.
- [69] G. Li, S. Chen, N. Pholchai, B. Reineke, P.W.H. Wong, E.Y.B. Pun, K.W. Cheah, T. Zentgraf, S. Zhang, Continuous control of the nonlinearity phase for harmonic generations, *Nat. Mater* 14 (6) (2015) 607–612.
- [70] W. Ye, F. Zeuner, X. Li, B. Reineke, S. He, C.-W. Qiu, J. Liu, Y. Wang, S. Zhang, T. Zentgraf, Spin and wavelength multiplexed nonlinear metasurface holography, *Nat. Comm.* 7 (2016) 11930.
- [71] F. Walter, G. Li, C. Meier, S. Zhang, T. Zentgraf, Ultrathin nonlinear metasurfaces for optical image encoding, *Nano Lett.* 17 (5) (2017) 3171–3175.
- [72] E. Almeida, O. Bitton, Y. Prior, Nonlinear metamaterials for holography, *Nat. Comm.* 7 (2016) 12533.
- [73] G. Li, S. Zhang, T. Zentgraf, Nonlinear photonic metasurfaces, *Nat. Rev. Mater.* 2 (2017) 17010.
- [74] X. Zhang, Z. Tian, W. Yue, J. Gu, S. Zhang, J. Han, W. Zhang, Broadband terahertz wave deflection based on C-shape complex metamaterials with phase discontinuities, *Adv. Mater* 25 (33) (2013) 4567–4572.
- [75] L. Liu, X. Zhang, M. Kenney, X. Su, N. Xu, C. Ouyang, Y. Shi, J. Han, W. Zhang, S. Zhang, Broadband metasurfaces with simultaneous control of phase and amplitude, *Adv. Mater* 26 (29) (2014) 5031–5036.
- [76] S. Fan, W. Suh, J.D. Joannopoulos, Temporal coupled-mode theory for the Fano resonance in optical resonators, *J. Opt. Soc. Am. A* 20 (3) (2003) 569–572.
- [77] Z.-L. Deng, J.-W. Dong, H.-Z. Wang, S.H. Cheng, J. Li, Power transmission and group delay in gain-assisted plasmon-induced transparency, *AIP Adv.* 3 (2013), 032138.
- [78] H.A. Haus, *Waves and Fields in Optoelectronics*, Prentice Hall, 1983.
- [79] A.E. Minovich, M. Peter, F. Bleckmann, M. Becker, S. Linden, A.V. Zayats, Reflective metasurfaces for incoherent light to bring computer graphics tricks to optical systems, *Nano Lett.* 17 (7) (2017) 4189–4193.
- [80] X. Zhang, J. Jin, M. Pu, X. Li, X. Ma, P. Gao, Z. Zhao, Y. Wang, C. Wang, X. Luo, Ultrahigh-capacity dynamic holographic displays via anisotropic nanoholes, *Nanoscale* 9 (4) (2017) 1409–1415.
- [81] C. Pfeiffer, A. Grbic, Metamaterial Huygens' surfaces: tailoring wave fronts with reflectionless sheets, *Phys. Rev. Lett.* 110 (19) (2013), 197401.
- [82] K. Chen, Y. Feng, F. Monticone, J. Zhao, B. Zhu, T. Jiang, L. Zhang, Y. Kim, X. Ding, S. Zhang, A. Alù, C.-W. Qiu, A reconfigurable active Huygens' met-alens, *Adv. Mater* 29 (17) (2017), 1606422-n/a.
- [83] I. Staude, A.E. Miroshnichenko, M. Decker, N.T. Fofang, S. Liu, E. Gonzales, J. Dominguez, T.S. Luk, D.N. Neshev, I. Brener, Y. Kivshar, Tailoring directional scattering through magnetic and electric resonances in subwavelength silicon nanodisks, *ACS Nano* 7 (9) (2013) 7824–7832.
- [84] J. Sautter, I. Staude, M. Decker, E. Rusak, D.N. Neshev, I. Brener, Y.S. Kivshar, Active tuning of all-dielectric metasurfaces, *ACS Nano* 9 (4) (2015) 4308–4315.
- [85] M. Decker, I. Staude, M. Falkner, J. Dominguez, D.N. Neshev, I. Brener, T. Pertsch, Y.S. Kivshar, High-efficiency dielectric Huygens' surfaces, *Adv. Opt. Mater* 3 (6) (2015) 813–820.
- [86] L. Wang, S. Kruk, H. Tang, T. Li, I. Kravchenko, D.N. Neshev, Y.S. Kivshar, Grayscale transparent metasurface holograms, *Optica* 3 (12) (2016) 1504–1505.
- [87] W. Zhao, H. Jiang, B. Liu, J. Song, Y. Jiang, High-efficiency beam manipulation combining geometric phase with anisotropic Huygens surface, *Appl. Phys. Lett.* 108 (18) (2016) 181102.
- [88] W. Zhao, H. Jiang, B. Liu, J. Song, Y. Jiang, C. Tang, J. Li, Dielectric Huygens' metasurface for high-efficiency hologram operating in transmission mode, *Sci. Rep.* 6 (2016) 30613.
- [89] K.E. Chong, L. Wang, I. Staude, A.R. James, J. Dominguez, S. Liu, G.S. Subramania, M. Decker, D.N. Neshev, I. Brener, Y.S. Kivshar, Efficient polarization-insensitive complex wavefront control using Huygens' metasurfaces based on dielectric resonant meta-atoms, *ACS Phot.* 3 (4) (2016) 514–519.
- [90] S.M. Kamali, E. Arbabi, A. Arbabi, Y. Horie, A. Faraon, Highly tunable elastic dielectric metasurface lenses, *Laser Photonics Rev.* 10 (6) (2016) 1002–1008.
- [91] A. Arbabi, Y. Horie, A.J. Ball, M. Bagheri, A. Faraon, Subwavelength-thick lenses with high numerical apertures and large efficiency based on high-contrast transmittarrays, *Nat. Commun.* 6 (2015).
- [92] A. Arbabi, R.M. Briggs, Y. Horie, M. Bagheri, A. Faraon, Efficient dielectric metasurface collimating lenses for mid-infrared quantum cascade lasers, *Opt. Express* 23 (26) (2015) 33310–33317.
- [93] E. Arbabi, A. Arbabi, S.M. Kamali, Y. Horie, A. Faraon, High efficiency double-wavelength dielectric metasurface lenses with dichroic birefringent meta-atoms, *Opt. Express* 24 (16) (2016) 18468–18477.
- [94] E. Arbabi, A. Arbabi, S.M. Kamali, Y. Horie, A. Faraon, Multiwavelength polarization-insensitive lenses based on dielectric metasurfaces with molecules, *Optica* 3 (6) (2016) 628–633.
- [95] E. Arbabi, A. Arbabi, S.M. Kamali, Y. Horie, A. Faraon, Controlling the sign of chromatic dispersion in diffractive optics with dielectric metasurfaces, *Optica* 4 (6) (2017) 625–632.
- [96] E. Arbabi, A. Arbabi, S.M. Kamali, Y. Horie, A. Faraon, Multiwavelength metasurfaces through spatial multiplexing, *Sci. Rep.* 6 (2016) 32803.
- [97] M.P. Backlund, A. Arbabi, P.N. Petrov, E. Arbabi, S. Saurabh, A. Faraon, W.E. Moerner, Removing orientation-induced localization biases in single-molecule microscopy using a broadband metasurface mask, *Nat. Phot.* 10 (7) (2016) 459–462.
- [98] A. Arbabi, E. Arbabi, Y. Horie, S.M. Kamali, A. Faraon, Planar metasurface retroreflector, *Nat. Phot.* 11 (7) (2017) 415–420.
- [99] A. Zhan, S. Colburn, R. Trivedi, T.K. Fryett, C.M. Dodson, A. Majumdar, Low-Contrast dielectric metasurface optics, *ACS Phot.* 3 (2) (2016) 209–214.
- [100] J. Lin, P. Genevet, M.A. Kats, N. Antoniou, F. Capasso, Nanostructured holograms for broadband manipulation of vector beams, *Nano Lett.* 13 (9) (2013) 4269–4274.
- [101] Z. Xie, T. Lei, G. Si, X. Wang, J. Lin, C. Min, X. Yuan, Meta-holograms with full parameter control of wavefront over a 1000 nm bandwidth, *ACS Phot.* 4 (9) (2017) 2158–2164.
- [102] Z.-L. Deng, S. Zhang, G.P. Wang, A facile grating approach towards broadband, wide-angle and high-efficiency holographic metasurfaces, *Nanoscale* 8 (3) (2016) 1588–1594.
- [103] Z.-L. Deng, S. Zhang, G.P. Wang, Wide-angled off-axis achromatic metasurfaces for visible light, *Opt. Express* 24 (20) (2016) 23118–23128.
- [104] Z.-L. Deng, X. Li, G.P. Wang, A Multifunctional Metasurface: from Extraordinary Optical Transmission to Extraordinary Optical Diffraction in a Single Structure, arXiv:1705.10171, 2017.
- [105] N.M. Estakhri, V. Neder, M.W. Knight, A. Polman, A. Alù, Visible light, wide-angle graded metasurface for back reflection, *ACS Phot.* 4 (2) (2017) 228–235.
- [106] Y. Ra'di, D.L. Sounas, A. Alù, Meta-gratings: beyond the Limits of Graded Metasurfaces for Wavefront Control, arXiv:1705.03879, 2017.
- [107] K. Huang, H. Liu, F.J. Garcia-Vidal, M. Hong, B. Luk'yanchuk, J. Teng, C.-W. Qiu, Ultrahigh-capacity non-periodic photon sieves operating in visible light, *Nat. Comm.* 6 (2015) 7059.
- [108] K. Huang, H. Liu, G. Si, Q. Wang, J. Lin, J. Teng, Photon-nanosieve for ultra-broadband and large-angle-of-view holograms, *Laser Photonics Rev.* (2017). 1700025-n/a.
- [109] Y.-Z. Liu, J.-W. Dong, Y.-Y. Pu, B.-C. Chen, H.-X. He, H.-Z. Wang, High-speed full analytical holographic computations for true-life scenes, *Opt. Express* 18 (4) (2010) 3345–3351.
- [110] X. Ni, A.V. Kildishev, V.M. Shalaev, Metasurface holograms for visible light, *Nat. Commun.* 4 (2013) 3807.
- [111] L. Huang, X. Chen, H. Mühlenbernd, H. Zhang, S. Chen, B. Bai, Q. Tan, G. Jin, K.-W. Cheah, C.-W. Qiu, J. Li, T. Zentgraf, S. Zhang, Three-dimensional optical holography using a plasmonic metasurface, *Nat. Commun.* 4 (2013) 2808.
- [112] L. Nikolova, P.S. Ramanujam, *Polarization Holography*, Cambridge University Press, 2009.
- [113] T. Todorov, L. Nikolova, N. Tomova, *Polarization holography. 1: a new high-efficiency organic material with reversible photoinduced birefringence*, *Appl. Opt.* 23 (23) (1984) 4309–4312.
- [114] D. Ilieva, L. Nedelchev, P. Ts, N. Tomova, V. Dragostinova, L. Nikolova, Holographic multiplexing using photoinduced anisotropy and surface relief in azopolymer films, *J. Opt. A Pure Appl. Opt.* 7 (1) (2005) 35.
- [115] T. Todorov, L. Nikolova, K. Stoyanova, N. Tomova, *Polarization holography. 3: some applications of polarization holographic recording*, *Appl. Opt.* 24 (6) (1985) 785–788.
- [116] K.Y. Bliokh, F.J. Rodriguez-Fortuno, F. Nori, A.V. Zayats, Spin-orbit interactions of light, *Nat. Phot.* 9 (12) (2015) 796–808.
- [117] Q. Guo, W. Gao, J. Chen, Y. Liu, S. Zhang, Line degeneracy and strong spin-orbit coupling of light with bulk bianisotropic metamaterials, *Phys. Rev. Lett.* 115 (6) (2015) 067402.

- [118] V.G. Sala, D.D. Solnyshkov, I. Carusotto, T. Jacqmin, A. Lemaître, H. Terças, A. Nalitov, M. Abbarchi, E. Galopin, I. Sagnes, J. Bloch, G. Malpuech, A. Amo, Spin-orbit coupling for photons and polaritons in microstructures, *Phys. Rev. X* 5 (1) (2015) 011034.
- [119] S. Xiao, J. Wang, F. Liu, S. Zhang, X. Yin, J. Li, Spin-dependent optics with metasurfaces, *Nanophotonics* 6 (1) (2017) 215.
- [120] M. Khorasaninejad, F. Aieta, P. Kanhaiya, M.A. Kats, P. Genevet, D. Rousso, F. Capasso, Achromatic metasurface lens at telecommunication wavelengths, *Nano Lett.* 15 (8) (2015) 5358–5362.
- [121] Z. Zhao, M. Pu, H. Gao, J. Jin, X. Li, X. Ma, Y. Wang, P. Gao, X. Luo, Multispectral optical metasurfaces enabled by achromatic phase transition, *Sci. Rep.* 5 (2015) 15781.
- [122] M. Pu, Z. Zhao, Y. Wang, X. Li, X. Ma, C. Hu, C. Wang, C. Huang, X. Luo, Spatially and spectrally engineered spin-orbit interaction for achromatic virtual shaping, *Sci. Rep.* 5 (2015) 9822.
- [123] Y. Li, X. Li, M. Pu, Z. Zhao, X. Ma, Y. Wang, X. Luo, Achromatic flat optical components via compensation between structure and material dispersions, *Sci. Rep.* 6 (2016) 19885.
- [124] M. Pu, X. Li, X. Ma, Y. Wang, Z. Zhao, C. Wang, C. Hu, P. Gao, C. Huang, H. Ren, X. Li, F. Qin, J. Yang, M. Gu, M. Hong, X. Luo, Catenary optics for achromatic generation of perfect optical angular momentum, *Sci. Adv.* 1 (9) (2015).
- [125] J. Cheng, H. Mosallaei, Truly achromatic optical metasurfaces: a filter circuit theory-based design, *J. Opt. Soc. Am. B* 32 (10) (2015) 2115–2121.
- [126] S. Wang, J. Lai, T. Wu, C. Chen, J. Sun, Wide-band achromatic flat focusing lens based on all-dielectric subwavelength metasurface, *Opt. Express* 25 (6) (2017) 7121–7130.
- [127] O. Avayu, E. Almeida, Y. Prior, T. Ellenbogen, Compos. Funct. Metasurf. multispectral achromatic Opt. 8 (2017), 14992.
- [128] K. Li, Y. Guo, M. Pu, X. Li, X. Ma, Z. Zhao, X. Luo, Dispersion controlling metalens at visible frequency, *Opt. Express* 25 (18) (2017) 21419–21427.
- [129] M. Khorasaninejad, Z. Shi, A.Y. Zhu, W.T. Chen, V. Sanjeev, A. Zaidi, F. Capasso, Achromatic metalens over 60 nm bandwidth in the visible and metalens with reverse chromatic dispersion, *Nano Lett.* 17 (3) (2017) 1819–1824.
- [130] X. Duan, S. Kamin, N. Liu, Dynamic plasmonic colour display, *Nat. Comm.* 8 (2017) 14606.
- [131] C. Yan, K.-Y. Yang, O.J.F. Martin, Fano-resonance-assisted metasurface for color routing, *Light Sci. Appl.* 6 (2017), e17017.
- [132] B.H. Chen, P.C. Wu, V.-C. Su, Y.-C. Lai, C.H. Chu, I.C. Lee, J.-W. Chen, Y.H. Chen, Y.-C. Lan, C.-H. Kuan, D.P. Tsai, GaN metalens for pixel-level full-color routing at visible light, *Nano Lett.* (2017), <https://doi.org/10.1021/acs.nanolett.1027b03135>.
- [133] D. Alfieri, G. Coppola, S. De Nicola, P. Ferraro, A. Finizio, G. Pierattini, B. Javidi, Method for superposing reconstructed images from digital holograms of the same object recorded at different distance and wavelength, *Opt. Comm.* 260 (1) (2006) 113–116.
- [134] S. Yeom, B. Javidi, P. Ferraro, D. Alfieri, S. De Nicola, A. Finizio, Three-dimensional color object visualization and recognition using multi-wavelength computational holography, *Opt. Express* 15 (15) (2007) 9394–9402.
- [135] T. Wang, Y. Yu, H. Zheng, Method for removing longitudinal chromatism in full color holographic projection system, *Opt. Eng.* 50 (9) (2011), 091302–091302-091305.
- [136] T. Kozacki, M. Chlipala, Color holographic display with white light LED source and single phase only SLM, *Opt. Express* 24 (3) (2016) 2189–2199.
- [137] S.-F. Lin, E.-S. Kim, Single SLM full-color holographic 3-D display based on sampling and selective frequency-filtering methods, *Opt. Express* 25 (10) (2017) 11389–11404.
- [138] Z. Zeng, H. Zheng, Y. Yu, A.K. Asundi, S. Valyukh, Full-color holographic display with increased-viewing-angle [Invited], *Appl. Opt.* 56 (13) (2017) F112–F120.
- [139] S. Choudhury, U. Guler, A. Shaltout, V.M. Shalaev, A.V. Kildishev, A. Boltasseva, Pancharatnam–berry phase manipulating metasurface for visible color hologram based on low loss silver thin film, *Adv. Opt. Mater.* 5 (10) (2017) 1700196.
- [140] A.E. Minovich, A.E. Miroshnichenko, A.Y. Bykov, T.V. Murzina, D.N. Neshev, Y.S. Kivshar, Functional and nonlinear optical metasurfaces, *Laser Photonics Rev.* 9 (2) (2015) 195–213.
- [141] Z. Miao, Q. Wu, X. Li, Q. He, K. Ding, Z. An, Y. Zhang, L. Zhou, Widely tunable terahertz phase modulation with gate-controlled graphene metasurfaces, *Phys. Rev. X* 5 (4) (2015), 041027.
- [142] P.C. Wu, N. Papasimakis, D.P. Tsai, Self-affine graphene metasurfaces for tunable broadband absorption, *Phys. Rev. Appl.* 6 (4) (2016) 044019.
- [143] L. Li, T. Jun Cui, W. Ji, S. Liu, J. Ding, X. Wan, Y. Bo Li, M. Jiang, C.-W. Qiu, S. Zhang, Electromagnetic reprogrammable coding-metasurface holograms, *Nat. Comm.* 8 (1) (2017) 197.
- [144] P.C. Wu, W. Zhu, Z.X. Shen, P.H.J. Chong, W. Ser, D.P. Tsai, A.-Q. Liu, Broadband wide-angle multifunctional polarization converter via liquid-metal-based metasurface, *Adv. Opt. Mater.* 5 (7) (2017) 1600938.
- [145] Q. Wang, E.T.F. Rogers, B. Gholipour, C.-M. Wang, G. Yuan, J. Teng, N.I. Zheludev, Optically reconfigurable metasurfaces and photonic devices based on phase change materials, *Nat. Phot.* 10 (1) (2016) 60–65.
- [146] A. Karvounis, B. Gholipour, K.F. MacDonald, N.I. Zheludev, All-dielectric phase-change reconfigurable metasurface, *Appl. Phys. Lett.* 109 (5) (2016) 051103.
- [147] C.H. Chu, M.L. Tseng, J. Chen, P.C. Wu, Y.-H. Chen, H.-C. Wang, T.-Y. Chen, W.T. Hsieh, H.J. Wu, G. Sun, D.P. Tsai, Active dielectric metasurface based on phase-change medium, *Laser Photonics Rev.* 10 (6) (2016) 986–994.
- [148] Y.-W. Huang, H.W.H. Lee, R. Sokhoyan, R.A. Pala, K. Thyagarajan, S. Han, D.P. Tsai, H.A. Atwater, Gate-tunable conducting oxide metasurfaces, *Nano Lett.* 16 (9) (2016) 5319–5325.
- [149] F. Zhou, Y. Liu, W. Cai, Plasmonic holographic imaging with V-shaped nanoantenna array, *Opt. Express* 21 (4) (2013) 4348–4354.
- [150] S. Sun, K.-Y. Yang, C.-M. Wang, T.-K. Juan, W.T. Chen, C.Y. Liao, Q. He, S. Xiao, W.-T. Kung, G.-Y. Guo, L. Zhou, D.P. Tsai, High-efficiency broadband anomalous reflection by gradient meta-surfaces, *Nano Lett.* 12 (12) (2012) 6223–6229.